Physics – Uspekhi **64** (3) 280 – 303 (2021)

REVIEWS OF TOPICAL PROBLEMS PACS numbers: 42.68.Bz, **47.27.–i**, 92.60.hn

Outer scale of turbulence and its influence on fluctuations of optical waves

V P Lukin

DOI: https://doi.org/10.3367/UFNe.2020.10.038849

Contents

Abstract. **Based on generalizations of numerous measurements and calculations, the influence of the low-frequency part of the atmospheric turbulence spectrum, directly adjacent to the inertial interval, on the statistical characteristics of fluctuations of optical waves propagating in the atmosphere is analyzed. The measured atmospheric turbulence spectra are compared with isotropic models. The outer scale of turbulence in the surface layer of the atmosphere is found to be dependent not only on the height above the underlying surface but also on the type of atmospheric stratification. The influence of the low-frequency part of the atmospheric turbulence spectrum on the phase fluctuations of optical waves propagating both along horizontal paths and obliquely through the entire atmosphere is analyzed.**

V P Lukin Zuev Institute of Atmospheric Optics,
Siberian Branch of the Russian Academy of Sciences,
pl. Akademika Zueva 1, 634055 Tomsk, Russian Federation
E-mail: lukin@iao.ru

Received 14 February 2020, revised 2 October 2020
Uspekhi Fizicheskikh Nauk **191** (3) 292 – 317 (2021)
Translated by M Sapozhnikov

Keywords: atmosphere, optical waves, turbulence, model, outer scale, propagation, remote sensing

1. Introduction

The propagation of optical waves strongly depends on the atmospheric inhomogeneity caused by regular refraction, aerosol and molecular absorption, and scattering, turbulence, and nonlinear effects [1–5]. The waves propagate successfully, as a rule, when the influence of these factors on them is minimal. The optimal choice of conditions for optical observations is a transparent atmosphere without clouds, when the influence of absorption and scattering can be minimized. Under such conditions, the propagation of optical waves is mainly affected by atmospheric turbulence.

Scattering of light by turbulent atmospheric inhomogeneities is one of the main distortion mechanisms of optical waves propagating in the atmosphere. Random spatiotemporal variations in the atmospheric refraction index [1–4] distort the structure of optical beams and images due to intensity and phase fluctuations of the waves and are manifested, in particular, in the blurring, jitter, and flickering of radiation-source images and also in the turbulent attenuation of the mean detected signal power.

The turbulent inhomogeneities of the refractive index of atmospheric air caused by variations in its density produced first and foremost by temperature fluctuations lead to random variations in the propagation direction of optical radiation [4, 5–8]. The turbulent inhomogeneities of the air density produce in the atmosphere transparent lens-like formations of different sizes without distinct boundaries with different refractive indices and different optical strengths [5, 7–12]. These formations, which are randomly produced and randomly oriented in the atmosphere due to their motion with respect to each other and their common motion, cause significant distortions in light beams and images. They also produce random variations in the radiation propagation direction, intensity, and energy redistributions in beam cross sections and plane waves, beam defocusing, and an increase in the light field concentration. Due to propagation of a light wave through a turbulent atmosphere [13], a detector will record the amplitude (intensity) and phase distribution as some realization of a random function.

2. Gas-dynamic description of turbulence

In turn, turbulence itself, in particular atmospheric turbulence, is a complex physical phenomenon studied using the fundamental laws of physics presented by hydrodynamic equations [7, 8] for continuous media describing the motion of gases and liquids. Therefore, as an introduction to the problem, we will formulate briefly in this section the main regularities characterizing the turbulent state of a gas or liquid.

Thus, it is known that the flow of liquid is described by the vector velocity field $\mathbf{u}(\mathbf{r}, t)$ and the scalar fields of thermodynamic characteristics of a medium: pressure $p(\mathbf{r}, t)$, density $\rho(\mathbf{r}, t)$, and temperature $T(\mathbf{r}, t)$, where $\mathbf{r} = \{x, y, z\}$. The physical properties of liquid (or gas) are determined from the values of molecular transport coefficients: dynamic viscosity coefficient μ, kinematic viscosity coefficient $v = \mu/\rho$, second viscosity coefficient ζ, thermal conductivity coefficient κ, the liquid heat capacity at constant pressure, and temperature conductivity coefficient $\chi = \kappa c_p^{-1} \rho^{-1}$. Because the velocity and pressure fields in laminar and turbulent liquid flows are described by functions that are the solutions of hydrodynamic equations under corresponding initial and boundary conditions [7, 8], the study of the appearance of turbulence requires the analysis of solutions of boundary problems for hydrodynamic equations, the so-called Navier–Stokes equations, with the appropriate initial and boundary conditions.

Reynolds showed back in 1883 [14, 15] that the liquid-flow regime passes to the turbulent one when Reynolds numbers Re exceed the critical value (usually, $10^2 - 10^3$). At the same time, specific conditions are known [16] when the laminar regime is preserved for $\mathrm{Re} \sim 10^4$ and above, and under atmospheric conditions Re takes values exceeding many times the critical value (for example, Re is estimated as $\sim 10^{11} - 10^{12}$ in [17]), which means that the atmosphere is, as a rule, in the turbulent state.

2.1 Statistical description of turbulence. A N Kolmogorov's statistical approach

During the turbulent motion of liquid or gas, it is in fact impossible to describe separately the time dependences of the velocity, temperature, and density fields of one individual flow. For this reason, the properties of moving liquids and gases are described using statistical approaches and methods based on investigations of already smoothed characteristics.

Reynolds, who was the founder of the turbulence theory, proposed to expand the fields of hydrodynamic quantities of a turbulent flow (for example, velocity [15]) to the averaged (over the time interval or spatial region) and pulsed components and to study dynamic equations for averaged quantities. However, the simple averaging of flows in time or space proved to be not very convenient in use.

The structure of statistical moments of hydrodynamic fields is the simplest in the case of homogeneous and isotropic turbulence, whose concept was introduced by Taylor in his statistical theory of turbulence [17]. Spatial homogeneity and isotropy require the absence of boundaries and a constant mean flow velocity. For this reason, this turbulence model is of little use for describing real turbulent flows [12], because it represents a mathematical idealization for the approximate description of some particular types of turbulent flows produced in aerodynamic tubes in laboratories.

Kolmogorov applied the statistic approach to the mechanics of turbulence. He studied the entire ensemble of possible turbulent flows instead of averaging individual hydrodynamic fields by using the obtained probabilistic mean values over the ensemble of analogous flows. In this case, the fields of characteristics of turbulence will be random functions of time and space, for which the mathematical apparatus of the random field theory can be applied [18–21].

Kolmogorov defined in [20] the locally homogeneous and locally isotropic turbulence and formulated an important hypothesis that the structure of turbulence in 'small enough regions' with a 'large enough Reynolds number' has the local homogeneity and local isotropy. This can be illustrated by the following definitions: random field $f(\mathbf{r})$ is locally homogeneous if "the distributions functions of a random quantity $f(\mathbf{r}_1) - f(\mathbf{r}_2)$) are invariant with respect to the displacements of a pair of points $\mathbf{r}_1$, $\mathbf{r}_2$"; a locally isotropic field is a locally homogeneous field in which "the distributions functions of the quantity $f(\mathbf{r}_1) - f(\mathbf{r}_2)$ are invariant with respect to rotations and mirror reflections of the vector $\mathbf{r}_1 - \mathbf{r}_2$" [7].

Kolmogorov formulated the first and second fundamental hypothesis of the similarity of turbulent flows for locally isotropic turbulence. According to the first hypothesis [20], the turbulence spectrum (the spectral energy density of turbulence) in the equilibrium interval (consisting of the inertial and viscosity intervals) is uniquely determined by quantities v and ε, where v is the kinematic viscosity coefficient and ε is the average energy dissipation rate per liquid unit mass. According to the second hypothesis [20], the turbulence spectrum in the inertial interval is uniquely determined by the quantity ε and is independent of ν [19]. Later, Kolmogorov formulated the third hypothesis about the lognormal distribution of the dissipation rate of energy ε_r averaged over a sphere with radius r.

The structural function for the velocity field in the form of the second-order moment $\overline{[\mathbf{u}(\mathbf{r}_1+\mathbf{r})-\mathbf{u}(\mathbf{r}_1)]^2}$ introduced by Kolmogorov [20] (the upper bar means statistical averaging) is now traditionally denoted by $D_{rr}(\mathbf{r})$. The function is called 'structural' by Obukhov [10], because the velocity difference $\delta\mathbf{u} = [\mathbf{u}(\mathbf{r}_1+\mathbf{r})-\mathbf{u}(\mathbf{r}_1)]$ was treated by Kolmogorov as the basic kinematic characteristic of the local structure of a turbulent flow used for deriving the stochastic characteristics of the local turbulence. This characteristic is 'local' because it reflects the influence of only pulsating vortices on a scale smaller than the characteristic scale of the specified local region. Because the difference $\delta\mathbf{u}$ characterizes the relative motion of one elementary liquid volume with respect to another, the longitudinal function is equal to the averaged square of the relative converging velocity of elementary liquid volumes at two points or to the velocity of their distancing from each other. The transversal structural function is equal to the square of the relative rotation and displacement velocity of two such volumes.

Kolmogorov called the quantity $\eta = \lambda = \nu^{3/4}/\varepsilon^{1/4}$ introduced by him [20] as the scale of the field of higher-order pulsations gradually decaying due to viscosity the "internal scale of turbulence" [23]; it is now traditionally denoted by l_0 and called the *Kolmogorov internal scale of turbulence*. The scale of "first-order pulsations" [20] was called the *turbulence scale* [21], while the "integrated turbulence scale" was called the *outer scale of turbulence* [13] and is now denoted by L_0.

The dissipation rate ε of turbulent energy characterizes the energy dissipated to the unit volume per unit time, i.e., reflects the average velocity of energy transition from a source in the low-frequency spectral region (from larger-scale vortices) to the high-frequency drain (to smaller vortices) [11] and characterizes turbulence on all scales [22]. In the stationary turbulence regime, ε is assumed equal to the energy transfer rate over the spectrum [7, 8, 11].

Based on the formulated similarity hypotheses, Kolmogorov and Obukhov made a number of important conclusions about the statistical characteristics of small-scale components of turbulence [7–12, 13, 20–21]. The main one is the 'two-thirds law' for the structural function

$$D(r) = C\varepsilon^{2/3}r^{2/3} \quad \text{from} \quad l_0 \ll r \ll L_0\,, \tag{1}$$

which gives expressions for structural functions of $D_{rr}(r)$, $D_T(r)$, and $D_n(r)$ of longitudinal velocity V, temperature T, and refractive index n:

$$\begin{aligned} D_{rr}(r) &= C_V^2 r^{2/3}(C_V^2 = C\varepsilon^{2/3})\,, \\ D_T(r) &= C_T^2 r^{2/3}(C_T^2 = C_\theta \varepsilon^{-1/3}N)\,, \\ D_n(r) &= C_n^2 r^{2/3}\,, \quad C_n^2 = \text{const}\, C_T^2\,, \end{aligned} \tag{2}$$

where C_V^2, C_T^2, and C_n^2 are the structural characteristics of V, T, and n, respectively, N is the temperature dissipation rate, and C and C_θ are the Kolmogorov and Obukhov constants, respectively, with numerical values $C = 1.9$ and $C_\theta = 3.0$ (with a 10% error) [5, 13]).

It is known that atmospheric turbulence (like any motion with dissipation) [8, 9] can be stationary only in the presence of energy sources. Energy in turbulent motion is supplied from external large-scale motions. These can be convective flows caused by Earth's heating, variations (displacements) in the velocity of the mean wind, and gravitational waves. These sources transfer energy to turbulence mainly through the energy interval in which the main energy of turbulence is concentrated. As a rule, the Reynolds number of the initial flow [8, 9] is large, resulting in a loss of its stability and the formation of vortices about the size of the initial flow playing the role of the outer scale L_0 of the turbulent motion. The turbulence energy is utilized in the dissipation interval, where the initial flow energy is transformed into heat under the action of viscosity forces. If the Reynolds number of the initial flow is large enough, the energy dissipation region is separated from the energy interval by the region of wave numbers κ satisfying the condition

$$L_0^{-1} \ll \kappa \ll l_0^{-1}\,, \tag{3}$$

called the inertial interval, where l_0 is the internal scale of turbulence.

The character of atmospheric turbulence in inertial interval (3) is completely determined by the dissipation rate of the turbulence energy and by an external parameter N characterizing sources. This leads to the Kolmogorov–Obukhov 'two-thirds law' for locally homogeneous and isotropic turbulence, to which the 'five-thirds law' corresponds in the spectral language [11]:

$$E(\kappa) = C_1\varepsilon^{2/3}\kappa^{-5/3}\,, \tag{4}$$

where $E(\kappa)$ is the one-dimensional spectral density of kinetic energy, $C_1 \approx 1.4$ [3, 4, 13], and κ the spatial wave number.

This is the general picture of turbulent motion according to Kolmogorov in the briefest presentation. The turbulence produced in this picture is called in the literature 'Kolmogorov turbulence' [12, 18, 22], and the corresponding energy spectrum is called the 'Kolmogorov spectrum'.

2.2 Optical characteristics of atmospheric turbulence

In the absence of cloudiness for a clear unclouded atmosphere, atmospheric turbulence most strongly affects the quality of images and the structure of propagating radiation beams. Atmospheric turbulence is described by numerous optical parameters, the most complete information on the structure of turbulent flows being contained in temperature fluctuation spectra.

The refractive index $n(\lambda)$ of air as a function of the radiation wavelength in the atmosphere differs from unity only in the fourth decimal point, and it can calculated in the spectral range from 0.2 to 20 μm by the expression

$$\big(n(\lambda)-1\big)\times 10^6 = \frac{77.6P}{T} + \frac{0.584P}{T\lambda^2} - 0.06P_{\text{w.v}} \tag{5}$$

using the known values of temperature T [K], atmospheric pressure P [mbar], and partial pressure $P_{\text{w.v}}$ of water vapor. According to [4, 6], expression (5) gives a relative error of measuring the refractive index of no more than 0.3%. Because the water vapor pressure in Earth's atmosphere in middle latitudes does not exceed 40–50 mbar, the contribution of water vapor to the refractive index in the optical wavelength range from 0.2 to 20 μm is small. Expression (5) is valid in 'transparency windows' of the atmosphere [1].

It is known that all the main parameters of the atmosphere are related by the equation of state of an ideal gas,

$$P = \frac{\rho R_0 T}{\mu} ,$$

where μ is the molecular weight, ρ is the density, and R_0 is the universal gas constant.

The air density in the atmosphere changes with height, which is produced regular refraction. At the same time, the main distorting factor in the atmosphere is undoubtedly temperature. Obukhov showed in [12] that, for the spectrum of the temperature field as a conservative and passive impurity, the 'five-thirds law' is also fulfilled. An estimate of the influence of the humidity and pressure on the refractive index in the optical range shows that they do not play any significant role.

Under the action of inertial forces, large vortices experience cascade decay into smaller and smaller vortices, until the influence of viscosity forces exceeds that of inertial forces. The internal scale l_0 of turbulence determines the minimal size of vortices still existing in the atmosphere of 'laminar cells' [7, 8]. In the case of vortices with smaller sizes, turbulent motions dissociate into heat. In the atmosphere near Earth's surface, $l_0 \sim 10^{-3} - 10^{-2}$ m [1, 3, 5, 22], while in aerodynamic tubes, l_0 is about a few tenths of a millimeter. The Monin–Obukhov scale L in the theory of a stratified (thermally layered) atmosphere corresponds to the thickness of the sublayer of dynamic turbulence [9–12] in which turbulence is mainly caused by dynamic factors [13]. The scale was determined from dimensionality considerations. The temperature stratification parameter (the Monin–Obukhov number) $\zeta = h/L$, where the height h above the underlying surface characterizes different stratification regimes: stable (the heat flow is directed downward), unstable (the flow is directed upward), and indifferent (the flow tends to zero) [7, 8].

Structural functions introduced by Kolmogorov [18–21] and Obukhov [12, 13] are used for the statistical description of fluctuations of temperature, the refractive index, velocity, and other characteristics. According to Kolmogorov hypotheses, the structural function for locally homogeneous and isotropic turbulence in the inertial interval is specified by the Kolmogorov–Obukhov 'two-thirds law' for the refractive index n:

$$D_n(r) = C_n^2 r^{2/3} \quad \text{for} \quad l_0 \ll r \ll L_0 , \tag{6}$$

where C_n^2 is the structural characteristic of the refractive-index field. At the same time, for temperature T, we have

$$D_T(r) = C_T^2 r^{2/3} \quad \text{for} \quad l_0 \ll r \ll L_0 , \tag{7}$$

where C_T^2 is the structural characteristic of the temperature field.

In this case, the structural characteristic C_n^2 for the refractive-index field for 'dry air' is related to the structural characteristic C_T^2 for the temperature field by the expression

$$C_n^2 = \frac{10^{-12}}{T^2} \left(\frac{77.6}{T} P + \frac{0.584 P}{T \lambda^2} \right)^2 C_T^2 . \tag{8}$$

Structural characteristics C_n^2 and C_T^2 change in the atmosphere in horizontal and vertical directions, which plays an important role in the propagation of electromagnetic and acoustic waves. As a rule, these changes are detected with metrological and acoustical devices.

The theory developed by Kolmogorov and Obukhov predicted the shape of the turbulence spectrum in the inertial interval of wave numbers (3). The corresponding spectrum for the refractive index of the atmosphere in the inertial interval has the form

$$\Phi_n(\kappa) \approx 0.033 C_n^2 \kappa^{-11/3} . \tag{9}$$

The correctness of this expression was confirmed in numerous experiments [3, 4, 6, 8, 9]. At the same time, the theory of spectra outside the inertial interval is absent at present. The results of numerous experimental and theoretical studies [3, 5] show that a change in the temperature of atmospheric air by 1 degree causes a change in the refractive index by about 10^{-6}. The random time pulsations of temperature at a fixed detection point have an amplitude of about a few tenths of a degree with a period of $10^{-3} - 10^{0}$ s. On horizontal paths over distances of about $10^2 - 10^3$ m, the amplitude of spatial fluctuations of temperature can be a few ten degrees.

3. Calculations of the statistical characteristics of fluctuations of optical waves propagating in a turbulent atmosphere

In this section, the main results of the modern theory of waves propagating in random media are presented. The theory is based on studies [3, 5] by the scientific schools of S M Rytov and V I Tatarskii using the results of the Kolmogorov–Obukhov theory for theoretical and experimental studies of fluctuations of optical waves propagating in a turbulent atmosphere.

Theoretical calculations are based on expressions (7) and (8) for the structural function of the field of the refractive index and temperature and their Fourier transform — spectral densities for calculations of statistical characteristics of optical-field fluctuations: the intensity, the behavior of the centers of gravity of laser beams and optical images, and other parameters of optical waves formed during the propagation of optical waves through a turbulent medium.

The Kolmogorov–Obukhov turbulence model became the main one for the development of the theory of optical waves propagating in a turbulent atmosphere. One of the most important achievements of this theory was the development of the so-called smooth-perturbation method [3, 5] for calculating statistical characteristics, in particular, the structural functions of intensity and phase fluctuations for an optical wave. Calculations performed for an initial plane optical wave in the smooth-perturbation approximation gave expressions for the structural intensity and phase functions of an optical wave propagating through a turbulent medium layer:

$$\left. \begin{array}{l} D_\chi(\rho) \\ D_{\mathrm{s}}(\rho) \end{array} \right\} = 4\pi^2 k^2 \int_0^X \mathrm{d}\xi \int_0^\infty \mathrm{d}\kappa \, \kappa \Phi_n(\xi, \kappa) \times \left[1 - J_0(\kappa\rho) \right] f_{\chi,\mathrm{s}}(\kappa, \xi) , \tag{10}$$

where X is the distance propagated by the optical wave in the turbulent medium, k in the wave number of optical radiation, and ρ is the distance between two observation points of the optical field. The correlation functions of intensity and phase fluctuations are described by the expression

$$\left.\begin{array}{l} B_\chi(\rho) \\ B_\mathrm{s}(\rho) \end{array}\right\} = 4\pi^2 k^2 \int_0^X \mathrm{d}\xi \int_0^\infty \mathrm{d}\kappa\, \kappa \Phi_n(\xi, \kappa) J_0(\kappa\rho) f_{\chi,\mathrm{s}}(\kappa, \xi)\,. \quad (11)$$

Functions

$$f_{\chi,\mathrm{s}}(\kappa, \xi) = \left[1 \mp \cos\left(\frac{\kappa^2(x-\xi)}{k}\right)\right] \quad (12)$$

entering expressions (10) and (11) are called spectral filtering functions for the intensity and phase. They determine the interval of the turbulence spectrum making the largest contribution to the intensity and phase fluctuations.

3.1 Calculations of the intensity fluctuations of optical waves propagating in a turbulent medium

Note that there is development of the Kolmogorov–Obukhov model (9) expanding the applicability of the spectrum for describing the so-called viscosity interval (i.e., the interval of inhomogeneity sizes depending on the medium viscosity; in this interval, the kinetic energy converts to heat) [4]:

$$\Phi_n(\kappa, \xi) = 0.033 C_n^2(\xi) \kappa^{-11/3} \exp\left(-\frac{\kappa^2}{\kappa_\mathrm{m}^2}\right), \quad (13)$$

$$\kappa_\mathrm{m} = \frac{5.92}{l_0}\,.$$

Note also that expressions (9) and (10) are written assuming that the turbulence spectrum is isotropic and can be described by model (13) in the entire infinite interval of inhomogeneities. The features of the behavior of the spectral filtering function for the intensity allow one to calculate its statistical characteristics in the entire infinite interval of turbulent inhomogeneities by using spectrum (13), because

$$f_\chi(\kappa, \xi) = 1 - \cos\left(\frac{\kappa^2(x-\xi)}{k}\right) \approx \frac{\kappa^4(x-\xi)^2}{k^2} \quad (14)$$

for small wave numbers κ. This circumstance allowed applying models (9) and (13) in the infinite spectral interval in calculations of intensity fluctuations. In this connection, the statistic characteristics of intensity fluctuations of an optical wave propagating through a turbulent atmosphere layer can be correctly calculated, even for a purely power law spectrum (9).

3.2 Calculations of the statistical characteristics of phase fluctuations of optical waves

At the same time, model (9) cannot be used to calculate the correlation function and dispersion of fluctuations for phase fluctuations. This is explained by the fact that, because of features in the behavior of functions (12), phase fluctuations are determined by the largest inhomogeneities of the turbulence spectrum, whereas intensity fluctuations are most sensitive to small inhomogeneities of the turbulence spectrum. For phase fluctuations, model (9) provides the calculation of only structural phase function (10). It was shown in [3–6] that refractive-index fluctuations during the propagation of optical waves in the atmosphere cause perturbations of the radiation phase, which are characterized by the structural function, defined for a plane wave as

$$D_\varphi(r) = 2.91 k_0^2 r^{5/3} \int_0^L C_n^2\big[h(z)\big]\,\mathrm{d}z\,. \quad (15)$$

Expression (15) takes into account the dependence of the structural constant C_n^2 on the height above Earth's surface, while the integral is calculated along the entire path length L.

By using the structural constant of the refractive index, the correlation scale for a plane wave in a turbulent medium (or the Fried radius [25]) was also introduced:

$$r_0 = \left\{0.423 k_0^2 \int_0^L C_n^2\big[h(z)\big]\,\mathrm{d}z\right\}^{-3/5}, \quad (16)$$

where k_0 is the wave number of optical radiation.

The use of this parameter simplifies the expression for the structural function of phase fluctuations to the form

$$D_\varphi(r) = 6.88 \left(\frac{r}{r_0}\right)^{5/3}. \quad (17)$$

The coherence radius r_0 is an important characteristic of an optical system, determining the aperture size (its diameter) within which distortions can be taken into account in the form of a uniform slope. The coherence radius r_0 characterizes the minimal distance at which the random phase difference of the wave front does not exceed π [25]. It is known that in the absence of an atmosphere the angular resolution of an optical system is determined by the ratio λ/D, where λ is the wavelength and D is the diameter of a transmitter (or a receiver), while, during observations through a random inhomogeneous medium, the angular size of the image of a point source is specified by the ratio λ/r_0.

Note that the measurement of intensity fluctuations of optical radiation is a simpler problem than the measurement of phase fluctuations. Because of this, the first optical studies of turbulence spectra in the atmosphere involved measurements of intensity fluctuations [14], which made possible the reconstruction of the turbulence spectrum in the dissipation interval [26–28].

Along with the study of intensity fluctuations of optical waves in a turbulent medium, attempts were made to investigate the behavior of phase fluctuations of optical waves. Phase measurements in the optical range in the atmosphere in a large dynamic range of the spatial scatter of observation points is a technically intricate problem [29]. For this reason, the structural functions of optical waves in the spatial scatter of observation points comparable to the height on ground-level atmospheric paths were reliably obtained in experiments only in the second half of the 1970s [30–34]. These data and also correlation functions of spatial-position fluctuations for the centers of gravity [6, 13] of horizontally spaced optical beams contradicted theoretical calculations [14] obtained using the purely power Kolmogorov–Obukhov model for the spectral density of refractive-index fluctuations in the atmosphere.

The influence of the outer scale on fluctuations of optical waves propagating in a turbulent atmosphere were first pointed out in publications [29–32]. Similar investigations were performed in fact simultaneously in the USA and Italy [33, 34]. The results of [30–34] suggest that the structural phase function for optical waves propagating in a turbulent atmosphere noticeably differs from a power dependence corresponding to the Kolmogorov model of the turbulence spectrum.

Note that, for the well-known Kolmogorov model [8, 9, 26] of the turbulence spectrum corresponding to the 'two-thirds law' (more exactly the 'two-thirds hypothesis') for the structural function of the atmospheric refractive index, of all the statistical characteristics of phase fluctuations of an optical wave, only the structural phase function can be correctly calculated, because the dispersion and the correlation function of fluctuations are not defined for this model because of the singularity in the behavior of the turbulence spectrum in the low-frequency region. However, this singularity in the behavior of the spectral density of atmospheric turbulence is not important in calculations [14, 26] of intensity fluctuations of an optical wave propagating in a turbulent medium, which is related to features of the behavior of spectral filtering functions (12).

4. Reconstruction of the spectral density of fluctuations of the atmospheric refractive index from optical measurements

The study of fluctuations of parameters of an optical wave propagating through a turbulent layer can be used to measure this turbulence, which resulted in the development of methods for remote diagnostics of atmospheric turbulence. Laser measurements of atmospheric-turbulence parameters offer a number of advantages, and this resulted in the extensive development of methods for laser probing atmospheric turbulence. In particular, optical measurements provide better stability and reliability of the obtained statistical data, because they involve by their nature the additional averaging of characteristics measured along the propagation path. This resulted in extensive recent studies of the structure of atmospheric turbulence based on analyses of fluctuations of optical waves propagating through a turbulent medium layer.

It is known that the parameters of a light wave propagating through a medium containing the inhomogeneities of the refractive index are distorted [14, 26]. These distortions give information on the characteristics of the inhomogeneities. Measurements can be performed remotely, without placing a detector at a point under study. Thus, a medium under study is not perturbed, and it is possible to investigate media into which detectors cannot be placed. Attempts to relate the results of measurements of fluctuations of parameters of an optical wave propagating through an atmospheric layer to atmospheric parameters involves some problems. First, it is necessary to find the relation between atmospheric parameters and experimental data in the form of an equation. Second, to extract information on the atmosphere from experimental data, a convenient mathematical apparatus is required. This problem is far from trivial, because quantities being measured are related to atmospheric parameters via integral equations. Thus, the problem involves solving integral equations. Analytic solutions of such equations can be found only in some cases of interest, and, as a rule, it is necessary to use numerical methods. And, finally, measurements should be complete and accurate enough.

The most developed method for measuring the energy spectrum of refractive-index fluctuation is the method of reconstructing the latter from measurements of the statistic characteristics of fluctuations of parameters of optical waves propagating through a turbulent atmosphere layer. When optical waves propagate in a turbulent atmosphere, with small relative fluctuations of the refractive index only weakly changing at distances of the order of the wavelength, pulsation spectra of the refractive index of the medium can be determined from the spectra and correlation functions of fluctuations of optical-wave parameters [14–26].

One should bear in mind that, in the case of light waves, the temperature turbulence and the similarity [26] of the fluctuation spectra of the refractive index and temperature are in fact always considered. Optical and acoustic methods of measuring characteristics of the atmospheric turbulence used in combination allow the efficient study of the local structure of turbulence.

4.1 Phase optical measurements of fluctuations of the atmospheric refractive index

In the study of the spectra of atmospheric turbulence by optical methods, the question arises as to the sensitivity of optical-wave parameters to the functional form $\Phi_n(\kappa)$ of the spectral density of the refractive-index fluctuations. The problem is how to select the characteristic of the optical wave that would be simply measured and maximally sensitive to the shape of the spectrum $\Phi_n(\kappa)$ in one spectral region or another of spatial frequencies κ of turbulent inhomogeneities.

The atmospheric turbulence spectrum even in the ground-level layer has a large dynamic range, with spatial scales of κ extending from a few meters to a few tenths of a millimeter. For this reason, due to the finite accuracy of optical measurements, the spectrum cannot be reconstructed from fluctuations of one of the parameters of the optical wave. Studies of the sensitivity of different parameters of optical waves to the shape of the turbulence spectrum in different spectral regions showed that characteristics related to the optical-wave phase are mainly determined by the low-frequency inhomogeneities of fluctuations of the refractive index, whereas radiation-intensity fluctuations are determined by the high-frequency region of the turbulence spectrum [4, 14]. In other words, measurements of fluctuations of the optical-wave phase can be used to study the energy interval of the turbulence spectrum, while measurements of intensity fluctuations are for studying the equilibrium interval containing the inertial and viscosity intervals of this spectrum [27–29].

The first attempts to calculate these fluctuation characteristics of optical waves in different isotropic models of the spectral density taking into account the deviation of the spectrum from a power law in the region of the outer scale of turbulence were made in [30–37]. However, the degree of the correctness of these models of the turbulence spectrum remained unclear. In this connection, attempts were made to reconstruct the two-dimensional spectrum of refractive-index fluctuations from the measurements of the structural phase function. One of the first such attempts was paper [37], in which the turbulence spectrum was reconstructed from experiments performed on a horizontal atmospheric path 110 m in length. The path height above the underlying surface was 1.5 m on average.

The phase fluctuations of an optical wave caused by atmospheric turbulence were measured in the following experiment. Radiation from a helium-neon laser was split into two identical collimated beams 2 cm in diameter. The distance between the beams (along the y-axis) was successively changed with a step $\Delta_y = 5$ cm up to the value $y_{\mathrm{m}} = 1.1$ m. The fluctuation of the phase difference between the centers of the two interfering beams was detected with a digital optical phasemeter [29]. The phase differences 50 s in duration (the sampling volume was 5000 counts) were used to estimate the structural phase function $D_{\mathrm{s}}(y)$.

Structural functions normalized to the value $D_{\mathrm{s}}(y_{\mathrm{m}})$ for the maximum spacing are shown in Fig. 1 for four measure-

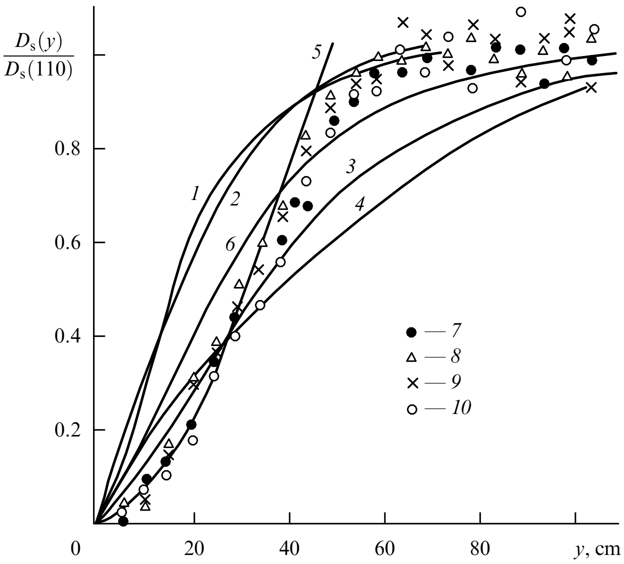

Figure 1. Normalized structural phase functions. Curves *1* and *3* are calculated using spectral model (26) (see Section 5): (*1*) $\kappa_{0K} = 6.5\ \mathrm{m}^{-1}$, (*3*) $\kappa_{0K} = 3.2\ \mathrm{m}^{-1}$. Curves *2* and *4* are calculated using spectrum (27): (*2*) $\kappa_{0R} = 26.5\ \mathrm{m}^{-1}$, (*4*) $\kappa_{oR} = 11.8\ \mathrm{m}^{-1}$. Curve *5* is described by function $ay^{5/3}$, where a is selected from the best fit with experiments. Curve *6* is selected from expression (31) for $\kappa_0 = 4.3\ \mathrm{m}^{-1}$. Different symbols are experimental data from [37].

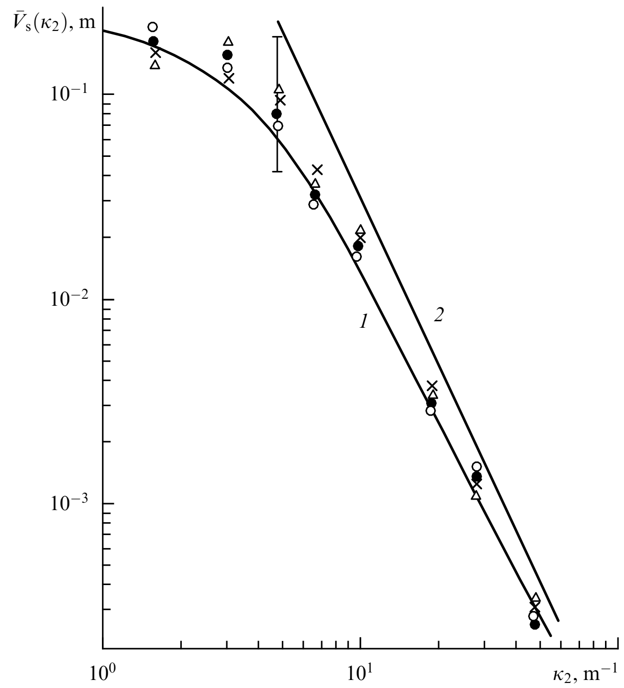

Figure 2. One-dimensional phase fluctuation spectrum reconstructed from data in Fig. 1. (*1*, *2*) Model spectrum (20) and the asymptotics form of this spectrum for $\kappa_0 = 4.3\ \mathrm{m}^{-1}$, respectively. Experimental points are denoted as in Fig. 1. The vertical bar shows the 80% confidence interval [37].

ment series. One can see that structural functions deviate from power dependence (15) and even saturate, tending to a constant level. Therefore, within the framework of the 'frozen' turbulence hypothesis [14, 32] within scales $y \approx V_\perp T$ ($V_\perp$ is the wind velocity component perpendicular to the path, $V_\perp \approx 2\ \mathrm{m\ s}^{-1}$ in experiments), phase fluctuations can be assumed to be homogeneous. The correlation coefficient for phase correlations was estimated from the expression

$$\hat{b}_s(y) = \begin{cases} 1 - \dfrac{D_s(y)}{D_s(y_m)}\,, & y \leqslant y_m\,, \\ 0\,, & y > y_m\,. \end{cases} \tag{18}$$

Using the representation [37] for the correlation function of phase fluctuations in the first approximation [14] of the smooth perturbation method, the spectrum of phase fluctuations caused by turbulence can be determined from the measured correlation coefficient of phase fluctuations (18). Figure 2 presents the one-dimensional spectral density of phase fluctuations $V_s(\kappa_2)$ calculated based on experimental measurements of the structural phase function $D_s(y)$ (see Fig. 1).

The results of this experiment were also discussed by comparing experimental data with the results of calculations in the isotropic Karman model [24, 36] for the spectral density $\Phi_n(0, \kappa_2, \kappa_3)$ of refractive-index fluctuations in the atmosphere taking into account a finite outer scale:

$$\Phi_n(0, \kappa_2, \kappa_3) = 0.033 C_n^2 (\kappa_0^2 + \kappa_2^2 + \kappa_3^2)^{-11/6}\,, \tag{19}$$

where $\kappa_0 = 2\pi/L_0$ is the wave number corresponding to the outer scale L_0 of turbulence and C_n^2 is the structural parameter [14, 26] of the refractive index.

Because the one-dimensional structural phase function (18) was measured in experiments, the one-dimensional spectrum of phase fluctuations $V_s(\kappa_2)$ was calculated using model (19):

$$V_s(\kappa_2) = 2\pi k^2 L V_n(0, \kappa_2)\,, \tag{20}$$

where $V_n(0, \kappa_2) = \int_0^\infty \mathrm{d}\kappa_3\, \Phi_n(0, \kappa_2, \kappa_3)$ is the one-dimensional spectrum of refractive-index fluctuations, $k = 2\pi/\lambda$, λ is the radiation wavelength, and L is the length of the uniform path.

Experimental and model phase-fluctuation spectra are compared in Fig. 2. The wave number $\kappa_0 = 4.3\ \mathrm{m}^{-1}$ corresponding to the outer scale for model spectrum (20) was chosen by a coincidence with experimental values at the maximum frequency point.

The normalized structural function corresponding to this spectrum is presented in Fig. 1 (curve *1*). Curve *2* in Fig. 1 corresponds to the Kolmogorov–Obukhov model,

$$\Phi_n(0, \kappa_2, \kappa_3) = 0.033 C_n^2 (\kappa_2^2 + \kappa_3^2)^{-11/6}\,, \tag{21}$$

when $\kappa_0 \ll \kappa_2$, $\kappa_0 \ll \kappa_3$.

One can see from Figs 1, 2 that the spectra and structural functions correspond as a whole to model (21). However, deviations of experimental functions from power dependences (curves *2* in Figs 1, 2) are observed at lower spatial frequencies (larger scales) than are model functions (curves *1* in Figs 1, 2). This means that, using the Karman model of the turbulence spectrum (19) to calculate the characteristics of optical waves, coincidence with experimental results can be expected only for a finite interval of the spatial and time scales.

4.2 Optical measurements of pulsation spectra of the refractive index in a convective flow

By analyzing the conclusions made in Section 4.1, note that measurements in [37] were performed in a real atmosphere containing both the convective component of turbulence and its dynamic component caused by variations in the mean wind. Theoretical estimates [8, 9, 26] show that it is natural to assume [38] that vertical convective motions in the atmosphere do not directly interact with the small-scale dynamic turbulence caused by the gradient of the mean velocity. Although dynamic turbulence produces vertical pulsations as well, their contribution to the total dispersion in the case of developed convection is negligibly small, and one can assume that vertical motions are caused only by convection. Thus, atmospheric turbulence should be considered [24–26] in the spectral respect as a sum of the convective and dynamic components. Therefore, separate studies of each of these components of turbulence are of interest.

Such studies of temperature-pulsation spectra [40] were performed in an artificially produced convective flow. The experimental setup for simulating conditions of purely thermal convection represented a heated surface 2×1 m^2 in size. Heating elements mounted above the surface produced conditions with different temperature gradients, the gradient value being determined by the current of heating elements. Such a regime of purely thermal turbulence in the absence of wind in a free atmosphere is realized in the case of unstable temperature stratification. Turbulence was studied using optical measurements.

In the case of homogeneous and isotropic fluctuations of the refractive index on a uniform atmospheric path (in the plane wave approximation), the statistical characteristics of fluctuations of optical waves $B(\rho)$ and the isotropic turbulence spectrum $\Phi_n(\kappa)\,(\kappa^2 = \kappa_2^2 + \kappa_3^2)$ are related by the expression

$$B(\rho) = \int_0^\infty \mathrm{d}\kappa\, \kappa f(\kappa, L) \Phi_n(\kappa) J_0(\kappa\rho)\,, \tag{22}$$

where ρ is the distance between observation points in a plane perpendicular to the light propagation direction, $f(\kappa, L)$ is the spectral filtering function determining the spectral region $\Phi_n(\kappa)$ making the main contribution to fluctuations of a given wave parameter (intensity or phase), and $J_0(\kappa\rho)$ is a Bessel function of the first kind.

It is shown in [37, 38, 40] that the solution of integral equation (22) for obtaining the turbulence spectrum from measurements of $B(\rho)$ in a finite interval of ρ values is a typical inverse problem [41]. To reconstruct the form of the function $\Phi_n(\kappa)$ in the inertial and energy intervals of wave numbers κ, it is necessary to measure simultaneously the intensity and phase fluctuations.

The experimental scheme for measuring phase fluctuations representing a two beams Michelson interferometer is described in [38, 40]. The interferometer base ρ (distance between the centers of beams) was changed from 1 cm to 50 cm. The phase difference between the centers of separated Gaussian beams was measured with an IFAS analog-digital phasemeter [29] with a threshold sensitivity of 0.1 rad. The intensity fluctuations were fixed on the axis of one of the beams.

The time correlation coefficients of the phase and intensity fluctuations of the optical wave were calculated from the data on synchronous realizations of a finite duration for the intensity and phase-difference fluctuations. The spectrum $\Phi_n(\kappa)$ was reconstructed from (22) by the set of correlation coefficients for a phase and intensity corresponding to the same realization. It is known that the turbulent regime [8, 9, 26] under convection has the property of self-similarity, i.e., the viscosity and temperature conductivity coefficients should not be determining parameters, and turbulent characteristics depend on the only parameter having the dimensionality of length — the height above the heated surface. Therefore, the study of refractive-index pulsation spectra in the flow produced as a function of the height above the heated surface is of interest.

For this purpose, the intensity and phase-difference fluctuations were measured for radiation propagating in a convective flow along a path 2 m in length. The path height above the underlying surface of a heater was successively 8, 14, and 21 cm. Radiation from a helium-neon laser was split into two identical collimated beams close in their structure to an infinite plane wave. The beams were separated from each other in the horizontal direction by the distance ρ. The mean floating velocity V of temperature air inhomogeneities was measured, which made possible moving from time correlation functions to spatial functions.

Figure 3 presents estimates of normalized correlation functions of intensity (Fig. 3a) and phase (Fig. 3b) fluctuations for different heights above the surface. Note that the correlation radius of phase fluctuations increases with increasing height, which can be interpreted as an increase in the outer scale L_0 with height, because, in the case of free convection, turbulent elements become larger with increasing height. The phase correlation function was measured in the

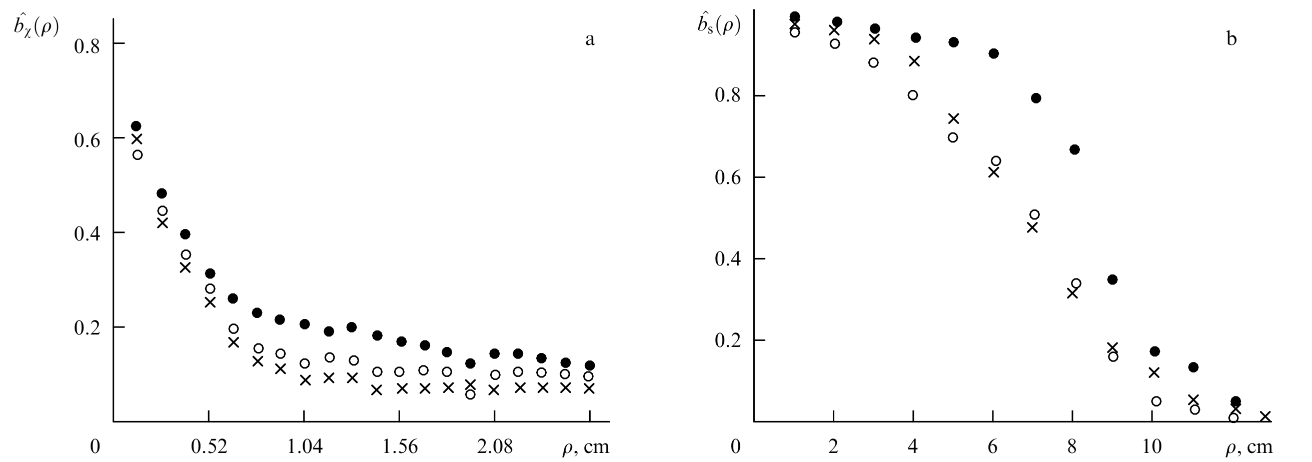

Figure 3. Normalized correlation functions of intensity (a) and phase (b) fluctuations for heights $h = 8$ cm (X's), 14 cm (circles), and 21 cm (dark dots) [40].

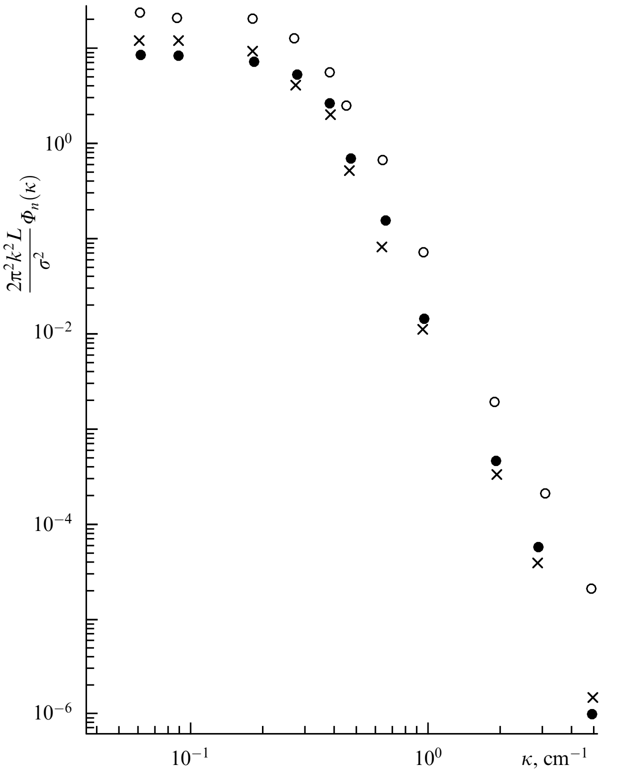

Figure 4. Reconstructed spectral density of refractive-index fluctuations at different heights [40] (notations as in Fig. 3).

range from 1 to 13 cm, which provided the reconstruction of the spectrum $\Phi_n(\kappa)$ for $0.08\ \text{cm}^{-1} \leqslant \kappa \leqslant 1\ \text{cm}^{-1}$. The intensity correlation was measured at 100 points with a step $\Delta = 0.026$ cm, the corresponding interval for the spectrum being $0.4\ \text{cm}^{-1} \leqslant \kappa \leqslant 20\ \text{cm}^{-1}$. Sewing the spectra reconstructed from data on the intensity and phase expanded the reliable-reconstruction interval compared to that in measurements of either intensity or phase fluctuations. Calculations showed that, for the 8% random measurement error of correlation coefficients (22), the turbulence spectrum was estimated in the interval $0.05\ \text{cm}^{-1} \leqslant \kappa \leqslant 20\ \text{cm}^{-1}$, with the error not exceeding the measured quantity.

Figure 4 presents the refractive-index pulsation spectra for different heights above the underlying surface. Each spectrum distinctly demonstrates two regions: the spectrum saturation region and the region where the behavior of the function $\Phi_n(\kappa)$ is described by a power law. The slope of the spectra is close to $-11/3$. The difference between spectra is most significant in the low-frequency region, which is explained by the monotonic increase in the outer turbulence scale with height [42].

The reconstructed spectra $\Phi_n(\kappa)$ obey a power law for κ up to 20 cm^{-1}, which means that the internal turbulence scale l_0 for this turbulent medium does not exceed a few millimeters.

4.3 Reconstruction of the turbulence spectrum from synchronous measurements of temporal amplitude and phase fluctuations in the atmosphere

The spatial correlation functions of phase fluctuations used in Sections 4.1 and 4.2 for the reconstruction of the turbulence spectrum require quite long measurements due to the necessity of changing the distance between interfering laser beams. However, the invariability of atmospheric characteristics during these measurements cannot be ensured in practice. This gave rise to the idea of reconstructing a spectrum from synchronous measurements of the spectra of temporal intensity and phase-difference fluctuations.

The study of this problem was initiated in the late 1970s [44] via the combined efforts of researchers at the Institute of Atmospheric Optics, Siberian Branch, Russian Academy of Sciences and the Institute of Atmospheric Physics, Russian Academy of Sciences. As initial equations, expressions for the spectra of time fluctuations of the intensity and phase of an optical wave propagating through a turbulent atmosphere layer were used. Based on results presented in [3, 4], we can obtain the equation

$$\omega W_\chi(\omega) = 2.6 C_n^2 k^{7/6} L^{11/6} X \int_X^\infty \mathrm{d}\kappa \left(1 - \frac{\sin\kappa^2}{\kappa^2}\right) \times \kappa^{-8/3}\left(\kappa^2 - X^2\right)^{-1/2} \varphi\left(\kappa D^{-1/2}\right), \tag{23}$$

relating the time spectrum of intensity fluctuations $W_\chi(\omega)$ with the function φ, which is a correction (characterizing the deviation from the Kolmogorov spectrum) to the one-dimensional power spectrum of the refractive-index field in the form

$$E_n(\kappa) \cong 0.4 C_n^2 \kappa^{-8/3} \varphi(\kappa\eta)\,; \tag{24}$$

here, $X = \omega\sqrt{L/k}/V$ is the dimensionless frequency, L is the length of an optical path in the atmosphere, k is the radiation wave number, V is the wind velocity across the light propagation direction, $D = L/(k\eta^2)$, C_n^2 is the structural parameter of the refractive index, $\eta = \nu^{3/4}\langle\varepsilon\rangle^{-1/4}$ is the Kolmogorov scale, ε is the dissipation rate of the turbulence energy, and ν is the kinematic viscosity of air.

The correction $\varphi(\kappa\eta)$ in the inertial spectral interval $E_n(\kappa)$ is identically unity and ensures the decay in the dissipation interval. The problem of spectrum reconstruction from optical measurements is reduced in fact to the determination of this function.

At the same time, to study the spectrum $E_n(\kappa)$ in the inertial and energy intervals, phase measurements are preferable [48, 65]. The corresponding equation

$$\omega W_{\delta s}(\omega) = 10.4 C_n^2 k^{7/6} L^{11/6} \sin^2\left(\frac{\rho}{2}\sqrt{\frac{k}{L}}X\right) \times X \int_X^\infty \mathrm{d}\kappa \left(1 + \frac{\sin\kappa^2}{\kappa^2}\right) \kappa^{-8/3}\left(\kappa^2 - X^2\right)^{-1/2} \varphi\left(\kappa D^{-1/2}\right) \tag{25}$$

relates the time fluctuation spectrum of the phase difference $W_{\delta s}(\omega)$ at points separated by the distance ρ in a plane perpendicular to the wave propagation direction to the function $\varphi(\kappa\eta)$. The phase-difference spectrum $W_{\delta s}(\omega)$ carries greater information on the spectrum $E_n(\kappa)$ in the region of small wave numbers than does $W_\chi(\omega)$. Because it is difficult to provide a high enough accuracy in measuring the phase difference in the high-frequency region [29, 30], the turbulence spectrum was reconstructed from synchronous measurements of both spectra and the combined solution of equations (23) and (25).

The mean velocity component V of the wind perpendicular to the path in equations (23) and (25) was determined by measuring the wind velocity and direction synchronously with optical measurements. Also, the structural constant C_T^2 of the temperature field was independently measured, because $C_n^2 \approx C_T^2 \langle \mathrm{d}n/\mathrm{d}T\rangle^2$ in the optical wavelength range [14].

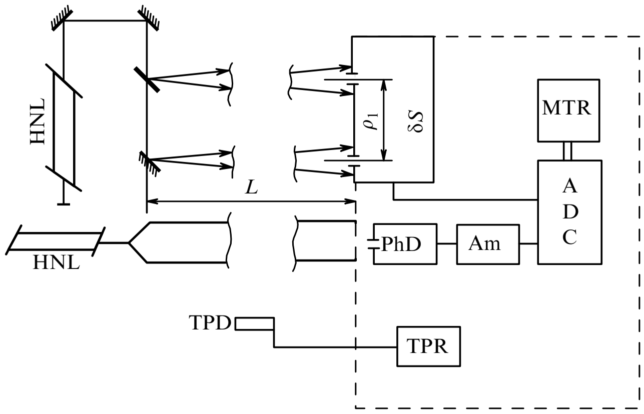

Figure 5. Block diagram of experiments. helium-neon laser (HNL); optical phasemeter (δS); photodetector (PhD), amplifier (Am), analog-to-digital converter (ADC); multichannel tape recorder (MTR); temperature pulsation detector (TPD); temperature pulsation recorder (TPR).

A block diagram of synchronous optical measurements [43, 44] is presented in Fig. 5. Measurements were performed in the steppe near the town of Tsimlyansk. Beams from a helium-neon laser propagated over a flat horizontal surface at a height of 1.5 m. The path length was 47 m. Amplitude measurements were performed using a broad collimated Gaussian beam 5 cm in diameter. Two other spatially separated identical beams parallel to the first beam were also formed. Fluctuations in the phase difference between the centers of interfering optical beams were detected in the detector plane with a phasemeter [29]. The phase difference was measured on bases of 55 and 5 cm. The fluctuations of the phase difference and amplitude logarithm were recorded with a sampling rate of 46 kHz.

The wind mean velocity and direction were measured with a cup anemometer and a rhumb meter mounted at a height of 1.5 m near the middle of the optical path. A detector for measuring temperature micropulsations was also placed here. C_T^2 was determined by measuring the mean square of temperature fluctuations at a fixed frequency of about 3 Hz.

Spectra $W_{\delta s}$ were calculated using recordings [43, 44] of phase-difference fluctuations 24 s in duration, while $W_\chi(\omega)$ were calculated from intensity fluctuations 8 s in duration. Figure 6 presents three experimental spectra of intensity fluctuations in the upper band of the figure; the lower band shows the corresponding phase spectra on bases ρ equal to 55 and 5 cm. Vertical bars in the figure show the scatter of experimental data. Figure 6 clearly demonstrates different sensitivities of $\omega W_\chi(\omega)$ and $\omega W_{\delta s}(\omega)$ to the refractive-index spectrum at different frequencies. Experimental data were processed by solving equations (23) and (25) together for the first time for the reconstruction of the turbulence spectrum in the entire frequency range. The vertical dashed line in Fig. 6 shows the value at which the reconstructed spectra were sewn.

Note that equations (23) and (25) are Abel integral equations. The solution of these equations using experimental data is an incorrect inverse problem requiring regularization [41, 45–47]. These equations were solved by the method of statistical regularization [45, 46].

Figure 7 shows the spectrum calculated by the measured values. In the region of small scales, the spectrum exhibits a sharp decay corresponding to the energy dissipation interval. Such a result was earlier obtained in [48].

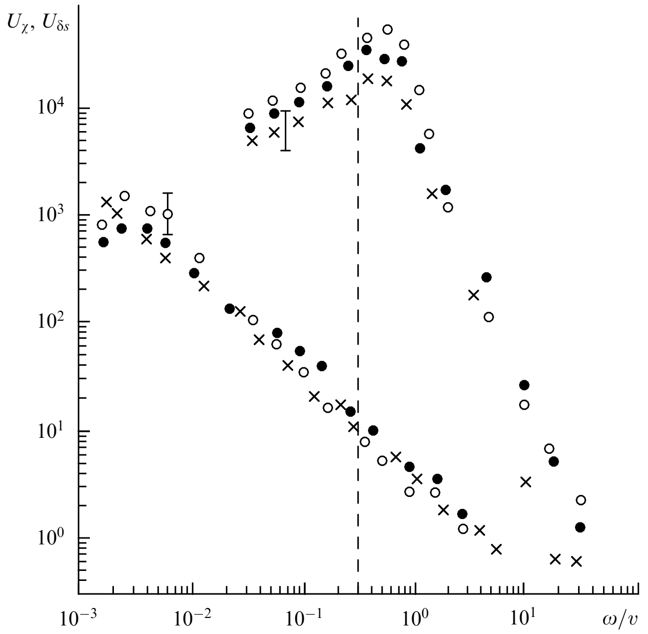

Figure 6. Dimensionless fluctuation spectra of light wave intensity logarithm $U_\chi = \omega W_\chi(\omega)/(2.6 C_n^2 k^{7/6} L^{11/6})$: upper experimental band; lower band is dimensionless phase-difference fluctuation spectra $U_{\delta s} = \omega W_{\delta s}(\omega)/(1.04 \times 10^{-6} C_n^2 k^{7/6} L^{11/6})$. Circles and X's correspond to measurements with bases $\rho = 55$ cm; dots are measurements with bases $p = 5$ cm; v is the transverse wing velocity [44].

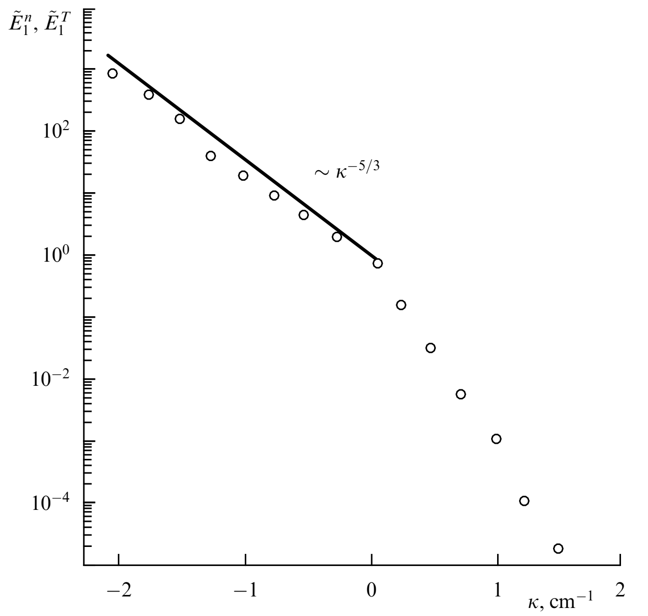

Figure 7. One-dimensional refractive-index spectrum reconstructed from experiments [44] (circles) and the one-dimensional temperature spectrum from [7, 8] (solid curve).

Combined measurements of the refractive-index spectrum [44] provided a significant improvement to the low-frequency region (compared to results [48]). In this frequency region, similar measurements of temperature spectra were performed with resistance thermometers [49, 50]. Refractive-index fluctuations in the optical range are mainly determined by temperature fluctuations, and therefore the shapes of spectra of these quantities can be compared. The solid curve in Fig. 7 shows the temperature spectrum [48] generalizing as series of measurements for small Richardson numbers (Ri = 0–2) [7, 8].

The method of optical measurements and data processing proposed in [43, 44] provided the reconstruction of the refractive-index spectrum in a very broad range of scales from 1.5 mm to 5 m, covering the energy, inertial, and viscosity intervals. These results also showed that, to describe the turbulence spectrum in the atmosphere correctly, one should take into account its deviations from the Kolmogorov–Obukhov model.

5. Analysis of low-frequency model spectra of atmospheric turbulence

In this section, different models of turbulence spectra using a finite size of the outer scale of turbulence are analyzed and compared. The aim is to select the most convenient and efficient model for theoretical calculations.

Analyses of the results of field measurements of atmospheric turbulence (see Figs 1 and 4) always gave rise to a natural question about the reasons for the deviation of the turbulence spectrum in the low-frequency region from the classical power shape.

The spectrum $E(\kappa)$ or the corresponding refractive-index pulsation spectrum $\Phi_n(\kappa)$ do not allow statistical characteristics of phase fluctuations of optical waves propagating in the turbulent atmosphere to be calculated, because the latter are determined by the behavior of the turbulence energy spectrum in the energy interval. At the same time, some experimental results, such as measurements of correlation and structural functions of phase fluctuations of optical waves [30–34], correlations of the displacement of the centers of gravity of spatially restricted Gaussian beams [35, 36], and direct measurements of the structural functions of temperature fluctuations [49, 50], demonstrate a significant deviation of real spectra $E(\kappa)$ (and corresponding spectra $\Phi_n(\kappa)$) from model (9) in the region of small κ.

Note, however, that measurements of the refractive-index (or temperature) pulsation spectra from fluctuations of optical waves propagating in the atmosphere showed in particular that the reconstructed refractive-index pulsation spectra are well described by the Karman model, taking into account the finiteness of the outer scale of turbulence [31, 44, 51].

5.1 Most popular models of the low-frequency spectrum of turbulence

The spectral density of refractive-index fluctuations $\Phi_n(\kappa)$ in the energy interval $\kappa < L_0^{-1}$, unlike that in the inertial interval of wavenumbers, is not a universal function [14, 51–55]. It was assumed in [8, 14, 38, 39, 49] that the low-frequency spectrum depends on both the underlying surface profile (for small heights) and weather conditions. The shape of a turbulence spectrum will change, of course, upon changing the height above the underlying surface and with variations in the degree of thermal stability of turbulence. Therefore, the assumption about the local homogeneity and isotropy of the turbulence spectrum may no longer be valid.

At the same time, the calculation of statistical characteristics of optical waves (estimates of fluctuation dispersions) requires fairly simple and convenient spectral models. At present, there are the following quite popular isotropic models of the spectrum $\Phi_n(\kappa)$, which take into account the deviation from a power law in the region of the outer scale of turbulence:

— the Karman model [24, 26, 30, 51],

$$\Phi_n(0,\kappa) = 0.033C_n^2\,(\kappa_{0\mathrm{K}}^2 + \kappa^2)^{-11/6}\,; \tag{26}$$

— the exponential model [36, 56, 57], which is sometimes called the 'Russian model',

$$\Phi_n(0,\kappa_2,\kappa_3) = 0.033C_n^2\kappa^{-11/6}\left[1-\exp\left(-\frac{\kappa^2}{\kappa_{0\mathrm{R}}^2}\right)\right]; \tag{27}$$

— and the Greenwood–Tarazano model [54],

$$\Phi_n(0,\kappa) = 0.033C_n^2\left(\frac{\kappa^2}{\kappa_{0\mathrm{G}}^2}+\frac{\kappa}{\kappa_{0\mathrm{G}}}\right)^{-11/6}. \tag{28}$$

Here, $\kappa_{0\mathrm{K}} = 2\pi/L_{0\mathrm{K}}$, $\kappa_{0\mathrm{R}} = 2\pi/L_{0\mathrm{R}}$, $\kappa_{0\mathrm{G}} = 2\pi/L_{0\mathrm{G}}$, $L_{0\mathrm{K}}$, $L_{0\mathrm{R}}$, and $L_{0\mathrm{G}}$ are the outer scales of models (26)–(28).

Naturally, models (26)–(28) only partially describe the behavior of the spectrum in the low-frequency region. In particular, these models behave differently in the low-frequency region, while their common feature is the presence of an inertial interval and the finiteness of the integral over the spectrum of the type $\int_0^\infty \mathrm{d}\kappa\,\kappa\Phi_n(0,\kappa)$. Therefore, the volume density of the turbulent energy for all these models is also finite. In addition, all these models correctly describe the inertial interval of the spectrum in which the type (9) power Kolmogorov dependence takes place.

In turn, the parameters of models (26)–(28), such as the structural parameter C_n^2 of the refractive index and the outer scale of turbulence L_0, can be described by independent models, for example, as a function of the height h above the underlying surface. In the literature, different models exist [58–66], describing the dependence of the structural parameter C_n^2 of the refractive index on the height. These models usually contain the following information:

— the characteristic value of the structural parameter C_n^2 of the refractive index of the atmosphere near Earth for the given area and its possible variations (daily and seasonal);

— the change in $C_n^2(h)$ with height h above the underlying surface;

— daily, seasonal, and other variations in the integrated value $\int_0^H \mathrm{d}h\,C_n^2(h)$ on vertical atmospheric paths with the height of the underlying surface up to some height H.

At the same time, information on the behavior of the outer scale L_0 of turbulence is quite limited. It is commonly assumed that the outer scale increases with height, $L_0 \sim h$, for small heights above the underlying surface in the case of convective turbulence [24, 65]. For heights h above 20 m, some authors, in particular Fried [42], recommend using the model $L_0 \approx 2\sqrt{h}$ (h and L_0 are measured in meters). For heights above 100 m, it is usually assumed that $L_0 = \mathrm{const}$. At the same time, measurements of $L_0(h)$ at the Observatoire de Haute Provence, France were approximated by the analytic formula [52]

$$L_0(h) = \frac{4}{1+\left[(h-8500)/2500\right]^2}\,, \tag{29}$$

while measurements at the La Silla Observatory, Chile [55] (belonging to the European Southern Observatory) were described by the similar expression

$$L_0(h) = \frac{5}{1+\left[(h-7500)/2000\right]^2}\,. \tag{30}$$

In these two models (29), (30), the height h is measured in meters.

There is also model [55] of the outer scale L_0, which uses the definition introduced in [14]. Of course, one should bear in mind that the outer scales in all these models should somewhat differ from each other, but undoubtedly they should be comparable.

5.2 Comparison of the parameters of turbulence-spectrum models with optical measurements

To compare models (26)–(28), it is reasonable to compare optical parameters measured using them. This was done for the first time using measurements of the structural phase function in [44]. The results are presented in Fig. 1, where models (26), (27), and Kolmogorov–Obukhov model (9) are compared. Models (26) and (27) were preliminarily used to calculate phase correlation coefficients $b_s(y)$, which are described by the expressions

$$b_s(y) = \frac{\Gamma(1/6)}{\pi} \left(\frac{y\kappa_{0K}}{2} \right)^{5/6} K_{-5/6}(y\kappa_{0K}) \,, \tag{31}$$

$$b_s(y) = \frac{{}_1F_1\left(-5/6, 1; \left(\dfrac{y\kappa_{0R}}{2} \right)^2 \right) - \left(\dfrac{y\kappa_{0R}}{2} \right)^{5/3}}{\Gamma(11/6)} \,, \tag{32}$$

respectively, where $K_{-5/6}(x)$ is the McDonald function and ${}_1F_1(\alpha, \beta; x)$ is the degenerate hypergeometric Gauss function.

Calculated and experimental correlation coefficients were compared in [44] (see Fig. 1) by selecting parameters κ_{0K} and κ_{0R} to obtain the best coincidence of the measured values of $D_s(y)/D_s(y_m)$ with the quantity $(1 - b_s(y))$ in the saturation region (curves *1*, *3*) and in the power-law region ($D_s(y) \sim y^{5/3}$) (curves *2*, *4*). Curve *5* corresponds to the calculated structural phase function for purely Kolmogorov model (9), i.e., to the function $ay^{5/3}$, where a is determined by the best fit of experimental data.

The comparison shows that models (26) and (27) as a whole well describe the behavior of the structural phase function; however, they cannot guarantee coincidence in the entire observation interval. For model (26), the best-fit outer scale L_{0K} (see Fig. 1) lies in the interval from 0.96 to 1.96 m. Thus, the most probable value of the outer scale is indeed comparable to the height 1.2–1.5 m above the underlying surface on which the measurements were performed in [44]. Recall that measurements in this study were performed on a horizontal atmospheric path over an even underlying surface.

5.3 Comparison of different models of the turbulence spectrum

The first attempts to compare calculations of the dispersion of the phase fluctuation of an optical wave in a turbulent medium in models (26)–(28), taking into account the finiteness of the outer scale of turbulence, were made in [67–73]. Note that these calculations were repeated later by researchers in Mexico [74], albeit without mentioning Russian studies [67–73].

In papers [67–69], several models of the two-dimensional spectral density $\Phi_n(0, \kappa)$ of fluctuations of the refractive index in the atmosphere were analyzed. The most popular, namely, the Karman model (26), the exponential model (27), and the Greenwood–Tarazano model (28), were compared with each other. Of course, the outer scales in these models were somewhat different. The models were compared [70, 71, 73] by calculating the dispersion of phase fluctuations of an optical wave propagating in the ground-level layer of a turbulent atmosphere. The initial expression used in calculations was the equation describing phase fluctuations of an optical wave propagating in a turbulent atmosphere in the smooth-perturbation approximation [14].

For simplicity of analysis, dispersions of phase fluctuations were compared for models (26)–(28) on a homogeneous atmospheric path. For these models, we have [71–73]

$$\langle S \rangle_K \approx \frac{12}{5} 0.033\pi^2 k^2 C_n^2 L \kappa_{0K}^{5/3} \,, \tag{33}$$

$$\langle S \rangle_R \approx \frac{12}{5} 0.033\pi^2 \Gamma\left(\frac{1}{6} \right) k^2 C_n^2 L \kappa_{0R}^{5/3} \,, \tag{34}$$

$$\langle S \rangle_G \approx 4\pi^2 0.033 \, \frac{\Gamma(1/6)\Gamma(5/3)}{\Gamma(11/6)} k^2 C_n^2 L \kappa_{0G}^{5/3} \,, \tag{35}$$

respectively. From the condition of the equality of dispersions of phase fluctuations calculated using different models,

$$\langle S \rangle_K = \langle S \rangle_R = \langle S \rangle_G \,, \tag{36}$$

we obtain mutual relations between their corresponding outer scales and their wave parameters for models (26)–(28):

$$\kappa_{0K}^{-1} = 2.84\kappa_{0R}^{-1} \,, \quad \kappa_{0K}^{-1} \approx 3.71\kappa_{0G}^{-1} \,, \quad \kappa_{0R}^{-1} \approx 1.32\kappa_{0G}^{-1} \,. \tag{37}$$

As a result, the calculations of optical characteristics performed in one spectral model can be reduced to another model using relation (37). Note here that Russian model (27) is the most convenient for performing analytic calculations. Calculations of parameters of optical waves for turbulence spectra with a finite outer turbulence scale useful for astronomers are presented in [73]. These results can be used for practical estimates.

6. Study of the anisotropy of atmospheric turbulence in the low-frequency spectral region

One of the most important properties of atmospheric turbulence is the continuity of motion when the refractive-index pulsations at each moment contain contributions from inhomogeneities of all scales. The largest inhomogeneities are caused by the decomposition of large-scale mean motions: zonal winds, atmospheric fronts, and inhomogeneities of the radiation regime. All these motions, decomposing due to instability, determine the spectrum of turbulent inhomogeneities. The region of large-scale inhomogeneities is most closely related to local meteorological parameters, first of all to the distributions of the wing velocity, temperature, and their gradients. For a ground-level layer, this region (with inhomogeneities of a size exceeding a few meters) is called the region of energy-producing vortices and is characterized, as a rule, by anisotropic properties, i.e., the properties of inhnomogeneities depend on the direction.

The correct description of phase fluctuations of optical waves now requires consideration of deviation of the atmospheric turbulence spectrum from the Kolmogorov–Obukhov power law in the region of low spatial frequencies [8, 9, 39, 70, 71]. At the same time, this region of the turbulence spectrum is the most poorly studied at present. It seems that one of the important properties of the turbulence spectrum in the low-frequency spectrum may be anisotropy.

The phase fluctuations of optical waves in the model of the spectral density of refractive-index fluctuations in the atmosphere can be calculated from the expression [67, 68]

$$\Phi_n(0,\kappa_2,\kappa_3) = 0.033C_n^2(X)(\kappa_2^2+\kappa_3^2)^{-11/6} \times \left[1-\exp\left(-\frac{\kappa_2^2}{\kappa_{02}^2}-\frac{\kappa_3^2}{\kappa_{03}^2}\right)\right], \tag{38}$$

where X is the coordinate along which the optical wave propagates, and κ_{02} and κ_{03} are the orthogonal spectral components of a two-dimensional wave vector corresponding to components of the outer scale size.

Model (38) is isotropic in the inertial interval of wavenumbers and can describe the anisotropy of the spectrum for unequal components ($\kappa_{02} \neq \kappa_{03}$) of the outer scale outside the inertial interval.

Among characteristics of optical waves propagating in the turbulence atmosphere, the most sensitive to the anisotropy of the turbulence spectrum are dispersions of the orthogonal components of random displacements of the center of gravity of the optical-source image being formed (or of the optical beam). Naturally, the properties of the corresponding statistical characteristics of optical waves also prove to be dependent on the direction.

Consider the features of random displacements of an optical image formed in the ground-level layer of the atmosphere on a horizontal atmospheric path. It is known that the position of the optical image of a remote source formed in the focal plane of an optical objective (lens) (radius R, focal distance F) is determined by the position of its center of gravity [4, 35, 75, 76],

$$\boldsymbol{\rho}_{\text{c.g.}} = \frac{\iint \mathrm{d}^2\rho\, \boldsymbol{\rho} I_F(\boldsymbol{\rho})}{\iint \mathrm{d}^2\rho\, I_F(\boldsymbol{\rho})}, \tag{39}$$

where $I_F(\boldsymbol{\rho})$ is the intensity distribution in the focal plane of the lens described by the expression [4, 5]

$$I_F(\boldsymbol{\rho}) = \frac{k^2}{4\pi^2F^2}\iint \mathrm{d}^2\rho_1\,\mathrm{d}^2\rho_2\, U(\boldsymbol{\rho}_1)U^*(\boldsymbol{\rho}_2) \times \exp\left[-\mathrm{i}\frac{k\boldsymbol{\rho}}{F}(\boldsymbol{\rho}_1-\boldsymbol{\rho}_2)\right], \tag{40}$$

where $U(\boldsymbol{\rho}_1)$ is the optical field propagating through a turbulent layer.

The integration in (39) is performed over the illuminated surface of the objective. Because image jitter is mainly caused by phase fluctuations, by disregarding amplitude fluctuations, we obtain the dispersion of displacement of the center of gravity $\langle\rho^2_{\text{c.g.}}\rangle$ in the form

$$\langle\rho^2_{\text{c.g.}}\rangle = \frac{F^2}{k^2\Sigma^2}\iint \mathrm{d}^2\rho\, \boldsymbol{\rho}\nabla^2 B_{\mathrm{s}}(\boldsymbol{\rho}). \tag{41}$$

Here, Σ is the area of the illuminated lens surface, $B_{\mathrm{s}}(\boldsymbol{\rho})$ is the correlation function of phase fluctuations of the optical wave $U(\boldsymbol{\rho})$, and the angle brackets mean averaging over the ensemble of fluctuations.

Using definition (39), we can write expressions for components of (ρ_y, ρ_z) of the image-jitter vector $\boldsymbol{\rho}_{\text{c.g.}}$. An estimate of the total dispersion $\langle\rho^2_{\text{c.g.}}\rangle = \langle\rho_y^2\rangle + \langle\rho_z^2\rangle$ and its components $\langle\rho_y^2\rangle$ and $\langle\rho_z^2\rangle$ is possible only when the correlation (or structural) function of phase fluctuations is known.

The results of calculations of these quantities were compared with experimental results [75–79]. The image-jitter dispersion in two mutually perpendicular directions $\langle\rho_y^2\rangle$ and $\langle\rho_z^2\rangle$ was studied with a tracking device [77] developed based on a coordinate-sensitive photodetector providing the simultaneous measurement of these dispersions. Experiments were performed for a model thermal turbulence [75–77] and in the real atmosphere [78–81].

Consider first of all the results in [75, 76] of a model experiment in which the setup generating a convective developed turbulence over a path 2 m in length described in Section 4.2 was used. Dispersions $\langle\rho_y^2\rangle$ and $\langle\rho_z^2\rangle$ related to image jitter were estimated from measurements for 100 s. The analysis of experimental data (Fig. 8) revealed a strong difference between the root-mean-square values of random displacements of the beam in the vertical, $\langle\rho_z^2\rangle$, and transverse, $\langle\rho_y^2\rangle$, directions, demonstrating the anisotropy of turbulence. Dispersions $\langle\rho_y^2\rangle$ and $\langle\rho_z^2\rangle$ were measured at several fixed heights (which corresponds to a change in z in Fig. 8) for different turbulence regimes. At small heights above the turbulence generator, the increase in the temperature gradient (with increasing thermodynamic instability) resulted in an increase in the difference between corresponding dispersions $\langle\rho_y^2\rangle$ and $\langle\rho_z^2\rangle$, i.e., the anisotropy of the spectrum increased. The elongation of the largest-scale inhomogeneities of the refractive index is probably maximal at small heights, and because of this the anisotropy of the medium is the most significant here. As the propagation height of optical waves increases, turbulence inhomogeneities become more isotropic, and dispersions $\langle\rho_y^2\rangle$ and $\langle\rho_z^2\rangle$ are equalized.

Such measurements on open atmospheric paths were performed in [75, 56] in Tsimlyansk and Tomsk. Measurements were performed on the scientific base of the Institute of Atmospheric Physics, USSR Academy of Sciences (Tsimlyansk) and on the scientific proving ground of the Institute of Atmospheric Optics, Siberian Branch, USSR Academy of Sciences (Tomsk). Optical measurements of fluctuations of the image jitter of an optical beam on a path 40.4 m in length (the propagation height of a laser beam was 1.15 m over the underlying surface) were accompanied by synchronous

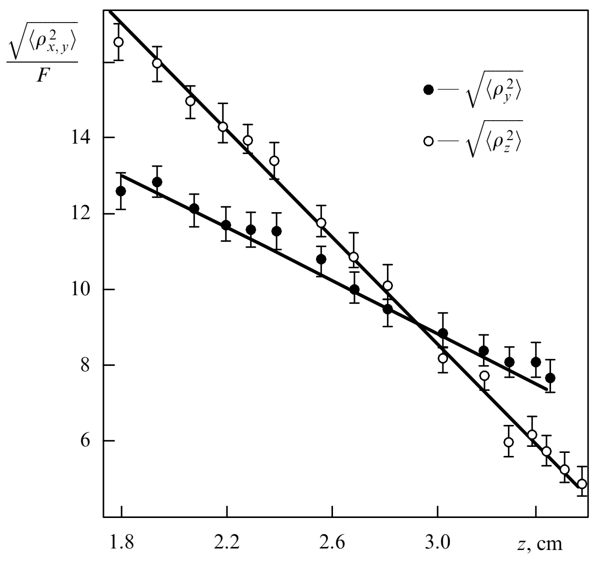

Figure 8. Height dependence of the root-mean-square deviation of a random beam deviation [75, 76].

measurements of temperature gradients and the vertical and transverse components of the mean wind velocity V_y and V_z. The processing of optical and metrological parameters measured in experiments gave the dispersions $\langle\rho_y^2\rangle$, $\langle\rho_z^2\rangle$ of radiation image jitter and the corresponding frequency fluctuation spectra W_y and W_z. The outer scale L_0 of turbulence and its components L_{0y} and L_{0z} can be estimated from the measured maximum position in spectra and the known components of the mean velocity V_y and V_z. In this case, L_{0y} and L_{0z} are the sizes of the outer scale in the vertical and transverse directions. The dispersion ratio $\langle\rho_y^2\rangle/\langle\rho_z^2\rangle$ characterizing the anisotropy of the turbulence spectrum in the low-frequency region changed from 1 to 2.1.

It was found in measurements [75, 76] that the quantity L_0 and its components L_{0y} and L_{0z} depended on the thermodynamic stability of the atmosphere. The outer scale L_0 of turbulence was calculated from these optical measurements to be from 4 to 1.25 m (the optical path length in these measurements was 1.15 m).

The results of synchronous meteorological measurements accompanying optical measurements were used to calculate the structural temperature parameter C_T^2, the vertical gradient of the mean temperature $(\Delta T/\Delta z)$, and then the outer scale $L_{0\,\mathrm{meteo}}$ from meteorological data using expression [14]

$$L_{0\,\mathrm{meteo}} = \left(\frac{C_T^2}{2.8(\Delta T/\Delta z)^2}\right)^{3/4}. \tag{42}$$

As a result, it was found that a comparison [75–79] of the optical measurements of L_0 and $L_{0\,\mathrm{meteo}}$ using expression (42) gives a high correlation, although a complete coincidence of L_0 and $L_{0\,\mathrm{meteo}}$ is absent.

Note that the corresponding components of the outer scale L_{0y} and L_{0z} were calculated from the measurements of positions of the maxima of frequency spectra $fW_y(f)$ and $fW_z(f)$ [81, 86] using the simple dependence

$$f_{\max} = \frac{\sqrt{3}V_{y,z}}{L_{0y,z}}, \tag{43}$$

where $f_{\max}$ is the position of the maximum in spectra fW_y and fW_z, V_y and V_z are components of the transverse wing velocity measured in experiments with a laser Doppler anemometer, L_{0y} and L_{0z} are components of the outer scale, and $L_0^2 = L_{0y}^2 + L_{0z}^2$.

In 1982, in the region of Zelenchukskaya stanitsa (at the top of the Semirodniki mountains near the Large Azimuthal Telescope), similar measurements were repeated on a horizontal track $L = 1685$ m, but under turbulent conditions at a height of about 2000 m above sea level. Also, the dispersions $\langle\rho_y^2\rangle$ and $\langle\rho_z^2\rangle$ of the random jitter of the optical source image were measured in two mutually perpendicular directions [79]. Optical measurements were accompanied by the measurements of meteorological parameters (temperature T and the mean wind velocity V). Image jitter was measured in the focus of a TT-600 telescope with a mirror diameter of 600 mm. The dispersion ratio $K = \langle\rho_y^2\rangle/\langle\rho_z^2\rangle$ was analyzed [79, 80].

The mean value of K proved to be 1.20 for small temperature gradients, i.e., the vertical random displacements of the image in fact coincide with horizontal displacements. For large temperature gradients and small wind velocities, anisotropy becomes stronger: $K = 2.89$. As the wind velocity increases, the anisotropy decreases to $K = 2.14$.

As a whole, experimental measurements in the ground-level atmospheric layer showed that image jitter anisotropy in this layer (at a height of $h \sim 1.5-3$ m) in fact always takes place [75–77]. This suggests a manifestation of the turbulence anisotropy. Note that such conclusions about the anisotropy of the turbulence spectrum were earlier made based on results in [82].

7. Relation between the outer scale of turbulence and variations in meteorological conditions

As mentioned in Section 5, atmospheric experiments revealed that the anisotropy of fluctuations of the position of an optical beam propagating through a turbulent medium layer depends on the varying meteorological conditions in the atmosphere [51–54]. Below, experiments verifying this conclusion are described.

Many studies on the turbulence theory [8, 9, 14, 16–18] reliably showed based on numerous experiments that the behavior of the turbulence spectrum of temperature or the refractive index of the atmosphere in the low-frequency region in the ground-level layer can no longer be described with the help of the only parameter — the turbulence intensity. It was also found that the assumption about the local isotropy for large-scale inhomogeneities close to the outer scale of turbulence is incorrect [4, 6, 13] for real atmospheric conditions.

7.1 Relation of the outer-scale to the thermodynamic stability parameter

Fluctuations of optical fields were calculated in different models [70–74] describing the spectrum at large scales. These models have two parameters, the second one being the so-called outer scale L_0. Different models of the turbulence spectrum were used in calculations, and the coincidence of experimental data with calculations was achieved by selecting the parameter L_0. Calculations showed that the outer scale proved to be comparable to the propagation height of the optical beam over the underlying surface [42, 65, 78]. However, the estimates of L_0 made by different authors [82–94] were significantly different.

This difference is probably explained as follows. In the real atmosphere, along with small-scale turbulence, larger-scale motions of a different nature are also present. They can be caused, for example, by the radiation variety of the underlying surface, the screening of the underlying surface by cloud structures, and a number of other factors. These large-scale formations can be considered in the ground-level layer as slow changes in external conditions determining the generation of small-scale turbulence. Note that parameters of turbulence (and its model parameters) in the ground-level layer should change with time with the characteristic scale of these large structures.

Therefore, if the model parameter L_0 is selected based on synchronous measurements of fluctuations of the optical-wave phase and the turbulence intensity C_T^2, it is necessary to also measure average meteoparameters. Experimental measurements [78] were performed for the homogeneous underlying surface on horizontal paths 15, 40, and 45 m in length with the propagation height of optical beams above the underlying surface of 1.2 m. The structural phase function [29] was measured for optical beams separated by the distance $\rho \approx 3$ m, i.e., when $D_s(\rho \to \infty) = 2\sigma_s^2$, where σ_s^2 is the phase-fluctuation dispersion in an infinite plane wave.

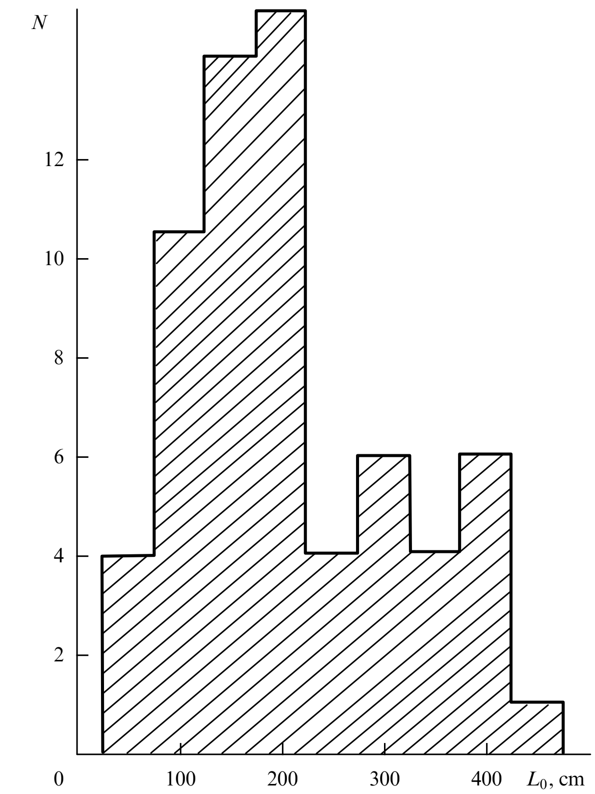

Figure 9. Histogram of the measured values of the outer scale for turbulence model (26) [78].

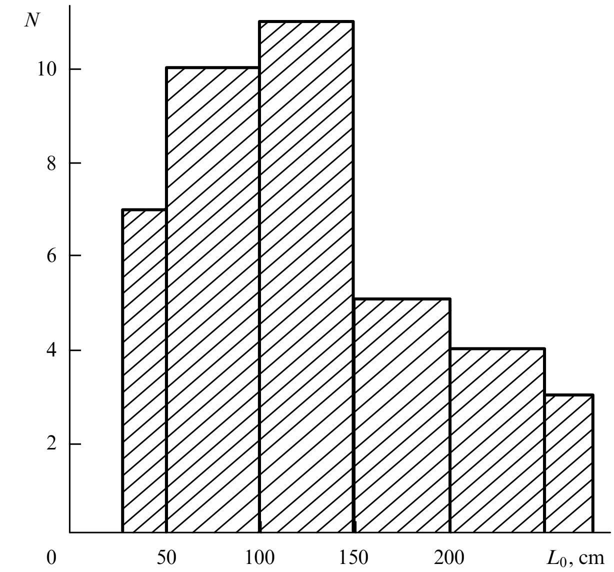

Figure 10. Histogram of the measured values of the outer scale for turbulence model (28) [78].

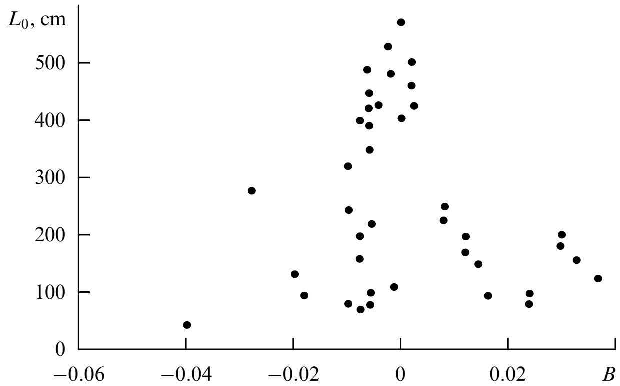

Figure 11. Variations of the average value of the outer scale of turbulence [78, 80] (measured at a height of 2.5 m above the underlying surface) as a function of Monin instability parameter (45).

Experimental data [78] were compared with the dispersion of phase fluctuations calculated in the smooth-perturbation approximation in the Karman model (26) of the turbulence spectrum and model (28). The outer scales L_0 for these models proved to be comparable.

According to calculations for model (26), we have

$$D_{\mathrm{s}}(\rho \to \infty) = 2\sigma_{\mathrm{s}}^2 = \frac{24}{5} 0.033\pi^2 k^2 C_n^2 L L_0^{5/3} \,. \tag{44}$$

Figure 9 presents a histogram of the measured values of L_0 characterizing the frequency of appearance of a certain value of an outer scale for model (26). Figure 10 shows a histogram of the distribution of the outer scale for model (28). A comparison of these two histograms shows that the Greenwood–Tarazino model (28) has lower values of the outer scale than the Karman model does (26).

Because the measurements of scales L_0 presented in Figs 9 and 10 were performed in changing meteorological conditions, an attempt was made in [78] to classify these measurements depending on the level of thermodynamic instability. For this purpose, the characteristic

$$B = \frac{gh\Delta T}{T\bar{V}^2} \tag{45}$$

was calculated from the measured average meteorological parameters, where $\Delta T = \bar{T}_2 - \bar{T}_{0.5}$ is the increment of the average temperature between levels 2 and 0.5 m above the underlying surface, T and $\bar{V}$ are the average absolute temperature and the wind velocity at height h, respectively, and g is the acceleration of gravity.

Characteristic (45) allows data in Figs 9 and 10 to be classified from the point of view of the thermodynamic stability. This is shown in Fig. 11. The values of L_0 exceeding the mean value proved to be realized for indifferent stratification, when $B = 0$. For unstable ($B < -0.01$) and stable ($B > 0.003$) stratifications, the values of L_0 that are lower than the average value are realized, which is quite explainable. Because a strong instability, i.e., large negative values of the parameter B correspond to the high breakup degree of the initial flow, the probability of a large value of L_0 appearing is small. For a large stability (large positive values of B), the initial flow proves to be weakly perturbed, and therefore there is a deficit of the inhomogeneities of all scales, including of the order of L_0. Finally, for values of B near zero (for indifferent stratification), the appearance of large scales is highly probable.

These results and conclusions based on them [78, 80, 83] were earlier widely discussed at international conferences, accepted by the world optical community, and later used for estimates of the efficiency of telescopes [73, 90, 95–98] with very large apertures.

At the same time, the classification of the values of L_0 (see Figs 9 and 10) determined from the measurements of the mean wind velocity shows that the smaller velocities correspond to the larger values of L_0 and vice versa. This confirms the conclusion [8–13] that the dynamic component of the turbulence is characterized by the smaller-scale structure rather than the convective component.

7.2 Measurement of the outer scale of turbulence in sediments

All measurements presented in Section 7.1 were made in a so-called pure atmosphere in the absence of sediments. However, a 'pure' atmosphere under real conditions is far from a given. In this connection, we consider here the change in the outer scale observed in [38] with the appearance of sediments in the atmosphere in the form of drizzle.

Note that changes in the structural phase function $D_s(\rho)$ of an optical wave propagating through an atmospheric layer were measured directly before the beginning of sediments and during their deposition. Figure 12 presents the results of two measurement series of $D_s(\rho)$ for virtually identical values of C_n^2. This is confirmed by the fact that the data of these two measurement series in fact coincide in Fig. 12 in the region of the power increase in $D_s(\rho)$ (straight line). However, the measurement data significantly differ in the region of $D_s(\rho)$ saturation.

Figure 12 shows that in a 'pure' atmosphere turbulence scales are greater than in a cloudy atmosphere (in the presence of sediments). This can be explained by the fact that, at the beginning of sediments and until a change in the turbulence regime, the directional motion of water particles in the sediments in fact 'breaks' large turbulent structures into smaller ones, resulting in a change of the turbulence spectrum in the region of large inhomogeneities.

Thus, numerous optical measurements in different regions showed that the turbulence spectrum in the ground-level atmospheric layer significantly deviates from the Kolmogorov–Obukhov spectrum in the region of scales comparable to the height above the underlying surface. It was found that isotropic models of the turbulence spectrum used in the theory to describe phase characteristics have certain restrictions. The low-frequency region of turbulent fluctuations is usually strongly anisotropic. It was found that both the absolute value and outer scale components in two mutually orthogonal directions were dependent on the atmosphere instability type. In addition, the presence of large aerosols (rain, drizzle, fog) in the atmosphere reduces the effective size of the largest turbulence scales.

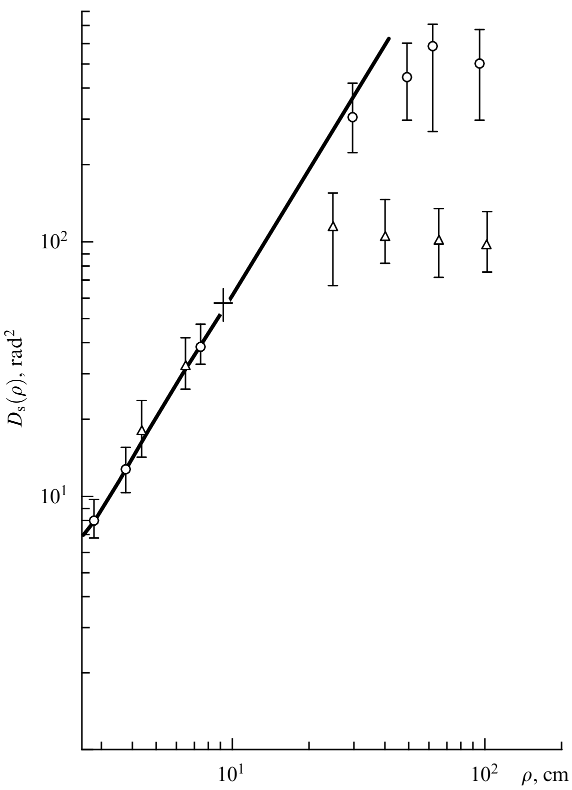

Figure 12. Structural phase function in a cloudy atmosphere (circles and triangles are measurements in 'pure' and cloudy atmospheres, respectively). Vertical bars show the scatter of experimental data [38].

One should bear in mind that these regularities observed for the low-frequency turbulence spectrum concern only the ground-level atmospheric layer. In the case of vertical or inclined atmospheric paths, it is necessary to additionally study the dependence of the outer scale on height. It seems that here the most useful ones may be astronomical measurements of image jitter for stars [1, 4, 5]. Section 8 is devoted to this question.

8. Study of atmospheric-turbulence dynamics based on astronomical observations

In this section, the influence of the outer scale on the data of astronomical observations is analyzed. A key point will be consideration of the possibility of introducing the effective outer scale of turbulence to describe phase distortions of an optical wave propagating in inhomogeneous vertical atmospheric paths as integral characteristics of the turbulence along the entire path. We will analyze preliminarily several known models of the height profile for the outer scale of turbulence and the structural characteristic of refractive-index fluctuations in the atmosphere for determining the effective outer scale. We will also study the influence of the change in the height profile by the effective outer scale on image parameters, in particular, we will estimate the error of Strehl ratio calculations for a telescope using the effective outer scale compared to the value obtained in calculations from the model height profile of the outer scale.

8.1 Effective outer scale of turbulence for the entire atmosphere

The possibility of introducing the effective outer scale to solve astronomical problems was considered in [60–68]. This is related to the fact that the projection of a large astronomical telescope requires the determination of its predicted characteristics based on limited information on parameters [60, 70–74, 79] of the height profiles of the atmospheric turbulence, such as the turbulence intensity C_n^2 and its outer scale L_0 in the assumed place of its location. The main characteristics of a telescope being projected are, as a rule, the point spread function (PSF) and the effective angular resolution.

One of the main traditional methods for estimating the angular resolution of a telescope is the measurement of the parameters of a star image (a long-exposure PSF) obtained in a small-diameter telescope. However, the turbulent PSF of a small telescope will correspond to the PSF of a larger-diameter telescope only when in both cases the outer scale of turbulence greatly exceeds the telescope diameter. It was shown in some experimental studies performed at various observatories [60–64] that this condition is violated in modern projects using telescopes with apertures of about 8–10 m (for example, VLT (Very Large Telescope) telescope-interferometers: 4 × 8 m, Keck: 2 × 10 m). Speaking of the outer scale, one should bear in mind that this parameter changes with increasing height, i.e., PSF simulation should use information on the parameters of the model of height profiles of atmospheric turbulence.

Therefore, of great interest is the possibility of introducing the so-called effective outer scale L_0^* as the integral characteristic of turbulence, which can be used in some problems to replace the height profile [83–89]. This characteristic is useful due to the limited application of height-profile models for atmospheric turbulence because of their dependence on the geographical location. This also considerably simplifies mathematical calculations taking into account the influence of atmospheric turbulence on the phase characteristics of an optical wave. Below, we consider a number of questions related to the introduction of the scale L_0^*, such as the fundamental possibility of using this characteristic, a class of problems where its application is reasonable, and the description accuracy. The influence of the replacement of the height profile by the effective outer scale on the image parameters is also studied and, in particular, the error of calculating the Strehl ratio of the turbulent PSF of a telescope using L_0^* is estimated in comparison with its value obtained by using the model height profile $L_0(h)$.

Studies were performed using semi-empirical profiles C_n^2 from [66] corresponding to the 'best' and the 'worst' visual conditions (astroclimate) and the following height-profile models $L_0(h)$:

$$\mathrm{B}: \quad L_0(h) = \begin{cases} 0.4, & h \leqslant 1 \text{ m}, \\ 0.4h, & 1 < h \leqslant 25 \text{ m}, \\ 2\sqrt{h}, & h > 25 \text{ m}, \end{cases}$$

$$\mathrm{C}: \quad L_0(h) = \begin{cases} 0.4, & h \leqslant 1 \text{ m}, \\ 0.4h, & 1 < h \leqslant 25 \text{ m}, \\ 2\sqrt{h}, & 25 < h < 1000 \text{ m}, \\ 2\sqrt{1000}, & h > 1000 \text{ m}, \end{cases} \tag{46}$$

$$\mathrm{D}: \quad L_0(h) = \frac{4}{1 + \left[(h - 8500)/2500\right]^2}\,,$$

$$\mathrm{E}: \quad L_0(h) = \frac{5}{1 + \left[(h - 7500)/2000\right]^2}\,.$$

Model B was proposed in paper [42]. Model C is the generalization and development of model B performed in [67–69], models D and E were obtained based on measurements performed in different regions of the world [62, 63].

Figure 13 presents vertical profiles corresponding to models (46). Figure 14 shows the vertical profiles of the turbulence intensity [66].

Different methods for determining the effective outer scale L_0^* were proposed in [83–86]. Thus, L_0^* can be determined by minimizing the integrated quadratic residual of structural functions of phase fluctuations of the form

$$\Delta\big(L_0, L_0(h)\big) = \int_0^{\rho_{\max}} \mathrm{d}\rho\, \rho \left[D_\varphi(\rho, L_0) - D_\varphi\big(\rho, L_0(h)\big)\right]^2, \tag{47}$$

where $D_\varphi\big(\rho, L_0(h)\big)$ is the structural function of phase fluctuations calculated using the height profile $L_0(h)$, $D_\varphi(\rho, L_0)$ is the structural phase function using a fixed (effective) outer scale $L_0 = \text{const}$, and $\rho_{\max}$ is the telescope aperture.

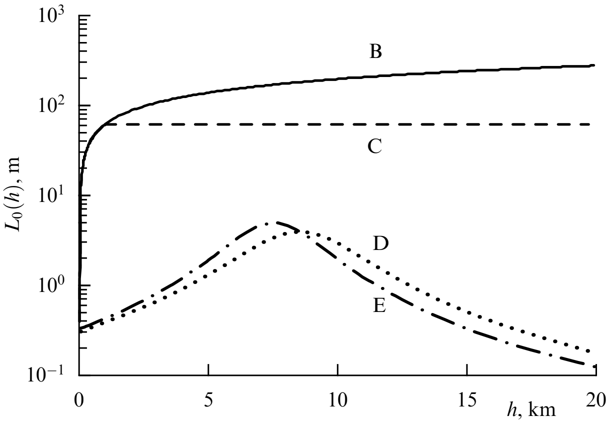

Figure 13. Models of vertical profiles (46) of the outer scale $L_0(h)$.

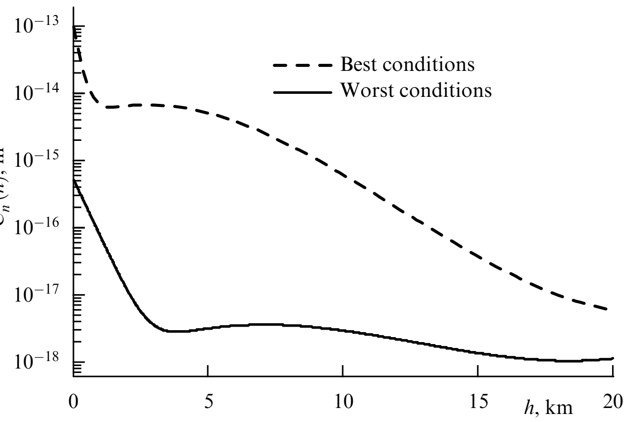

Figure 14. Vertical profiles [66] of the turbulence intensity $C_n^2(h)$.

Residual (47) determines the discrepancy of two structural functions. It was proposed to call the effective outer scale of the atmospheric turbulence the value of L_0^* at which the residual $\Delta(L_0, L_0(h))$ of the form (47) is minimal. Note that the upper integration limit in (47) in the method proposed is equal to $\rho_{\max}$. In papers [83–86], several different cases were studied, in particular, $\rho_{\max} = 10$ m, which corresponds to the aperture of a large telescope, and $\rho_{\max} = \infty$.

Table 1 presents the values of L_0^* determined by several methods for different models of $L_0(h)$ and $C_n^2(h)$.

The dependence of the effective outer scale L_0^* on the profile $C_n^2(h)$ shows that the smaller value of L_0^* for the 'best' conditions from the point of view of turbulence is caused by significant differences in the behavior of $C_n^2(h)$. Figure 14 shows that the 'best' $C_n^2(h)$ profile rapidly decreases with height, and the probability of large-scale fluctuations appearing decreases, which results in a decrease in $D_\varphi(\rho, L_0)$ and in the effective outer scale L_0^*.

Table 1. Effective outer scale L_0^* for $L_0(h)$ (48) and $C_n^2(h)$ [66] models.

Model $L_0(h)$	'Best' profile $C_n^2(h)$		'Worst' profile $C_n^2(h)$	
	0–10 m	0–∞	0–10 m	0–∞
B	34.7	58.4	55.4	98.0
C	32.5	42.9	40.6	52.3
D	0.60	0.71	1.04	1.78
E	0.68	0.84	1.31	1.56

The considerable difference between L_0^* values for the $L_0(h)$ models C and D can be explained as follows. A characteristic feature of model D is the presence of a finite maximal value of L_0 and its subsequent decrease at heights above 7–8 km (see Fig. 13), which, in fact, makes impossible the appearance of greater scales. At the same time, in model C in (46) the value of L_0 increases with height, which enhances the influence of large-scale fluctuations, and therefore an increase in $D_\varphi(\rho, L_0)$ can be expected, resulting in a corresponding increase in the effective outer scale L_0^*.

Note that similar estimates of the effective outer scale of atmospheric turbulence were earlier made in papers [87–89] using the expression

$$L_0^* = \left(\frac{\int_0^\infty \mathrm{d}h\, L_0^{5/3}(h) C_n^2(h)}{\int_0^\infty \mathrm{d}h\, C_n^2(h)} \right)^{3/5} \tag{48}$$

characterizing the dependence of the dispersion of phase fluctuations on the outer scale.

As a whole, note that, although this problem attracts great interest [90–114], information on the dependence of the outer scale on the height is quite limited at present.

8.2 Influence of the effective outer scale on the calculation characteristics of an image

The influence of the outer scale on the characteristics of optical systems in a turbulent atmosphere was studied in many papers [73, 74, 78, 87–89, 91–98]. In particular, the decrease in the calculated Strehl ratio was studied for astronomical telescopes taking into account the finiteness of the outer scale of turbulence. It is known that the turbulent broadening of an image reduces the peak intensity [91–98]. The Strehl ratio SR is determined by the ratio of the peak intensity I_{turb} of the turbulent image to the peak intensity I_{diff} of the diffraction image. If the structural function $D_\varphi(\rho)$ of phase fluctuations is known, the SR can be directly calculated [42, 72–74] from the expression

$$\mathrm{SR} = \frac{I_{\mathrm{turb}}}{I_{\mathrm{diff}}} = \frac{\int_0^D \mathrm{d}\rho\, \rho \tau_0(\rho) \exp\left(-1/2 D_\varphi(\rho)\right)}{\int_0^D \mathrm{d}\rho\, \rho \tau_0(\rho)}\,, \tag{49}$$

where D is the telescope diameter and $\tau_0(\rho) = (2/\pi)\{\arccos(\rho/D) - (\rho/D)[1-(\rho/D)^2]^{-1/2}\}$ is the diffraction-limited optical transfer function of the telescope.

For a homogeneous propagation path, i.e., when L_0 is independent of the height above the underlying surface, the SR ratio can be easily measured from the known telescope diameter D, the coherence radius r_0, and the value of L_0. Strehl ratios calculated for the homogeneous path are presented in Fig. 15. It can be seen that the SR decreases with increasing L_0, i.e., the increase in L_0 results in an increase in image distortion caused by the turbulent atmosphere.

Considering the SR dependence on the ratio D/r_0, note that the increase in D/r_0 for fixed D indicates an decrease in the coherent part of the aperture, which in turn reduces the peak intensity of the turbulent image. For the inhomogeneous path, the SR calculation is complicated, because the quantity L_0 in $D_\varphi(\rho)$ depends on the height. However, the entire atmospheric path can be divided into layers greater than L_0 in size, within which L_0 can be assumed constant. Assuming that correlations of turbulent fluctuations between such layers are absent in fact [14, 98–100], the total structural function can be calculated as the sum of structural functions of each layer.

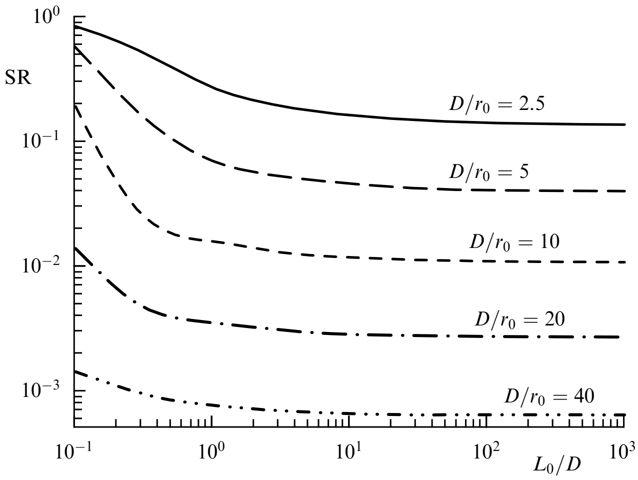

Figure 15. Strehl ratio for a homogeneous turbulent path [83, 85].

Using the obtained values of L_0^*, we can calculate the relative error of measuring the Strehl ratio $\varepsilon = (\mathrm{SR} - \mathrm{SR}^*)/\mathrm{SR}$, where SR is the Strehl ratio for the turbulent PSF calculated using the profile $L_0(h)$, and SR^* is the Strehl ratio calculated using L_0^*. The quantity ε determines the accuracy of predicting turbulent image distortions when the height profile is replaced by a finite value.

Summing up the results of studies [95–98], we can make some conclusions:

(i) The effective outer scale of turbulence can be introduced as an integral characteristic describing the atmospheric turbulence along an inhomogeneous atmospheric path.

(ii) The introduction of the effective outer scale can significantly simplify mathematical calculations of the influence of the atmospheric turbulence on the phase characteristics of an optical wave propagating along vertical and weakly inclined atmospheric paths.

(iii) Studies of the description accuracy showed that the error caused by the replacement of the height profile of the outer scale by a constant value — the effective outer scale — highly depends on both the height-profile model and the measuring method.

(iv) When the effective outer scale exceeds the telescope diameter, the error of measuring the Strehl ratio caused by the use of the effective outer scale instead of the profile will not exceed 16% on average.

8.3 Calculation of image jitter for an optical source in a random medium with a finite outer scale

Numerous experimental studies in the atmosphere [100–116] show that it contains regions where the turbulence significantly differs from the well-known Kolmogorov turbulence traditionally used for the description [10–13]. One of the possible reasons is the influence of the finiteness of the outer scale of turbulence. This question is important, for example, for problems related to terrestrial astronomy.

It is known that the random displacement of the center of gravity of the image from a remote optical source, for example, a star forming a plane wave front, is characterized by the position $\boldsymbol{\rho}_F^{\mathrm{pl}}$ of the energy center of gravity, which, in the first approximation, by ignoring amplitude fluctuations, is described by the expression [4, 5]

$$\boldsymbol{\rho}_F^{\rm pl} = -\frac{F}{k\Sigma}\iint_{\Sigma} \nabla S(\boldsymbol{\rho}_1)\,\mathrm{d}^2\rho_1\,. \tag{50}$$

In the geometrical optics approximation, the gradient of phase fluctuations $\nabla S(\boldsymbol{\rho}_1)$ for a plane wave can be written in the form

$$\nabla S(\boldsymbol{\rho}_1) = \mathrm{i}\int_0^X \mathrm{d}\xi_1 \iint \mathrm{d}^2\boldsymbol{\kappa}_1\, n(\boldsymbol{\kappa}_1, X-\xi_1)\boldsymbol{\kappa}_1 \exp(\mathrm{i}\boldsymbol{\kappa}_1\boldsymbol{\rho}_1)\,, \tag{51}$$

where F is the focal distance of the optical system, X is the distance propagated by an optical wave in a turbulent atmosphere, $n(\boldsymbol{\kappa}_1, X-\xi)$ is the two-dimensional spectral density of the expansion of fluctuations of the atmospheric refractive index, and k is the radiation wavenumber.

Then, similarly to calculations [4, 14], we obtain expressions for the calculations of the jitter of the image center of gravity in the form of an integral over the turbulence spectrum $\langle(\boldsymbol{\rho}_F^{\rm pl})^2\rangle$:

$$\left\langle(\boldsymbol{\rho}_F^{\rm pl})^2\right\rangle = 2\pi^2F^2\int_0^X \mathrm{d}\xi \iint \mathrm{d}^2\kappa\,\kappa^2\Phi_n(\boldsymbol{\kappa},\xi) \times \exp\left(-\frac{\kappa^2R^2}{2}\right). \tag{52}$$

To calculate integrals in (52), it is necessary to select one model or another of the turbulence spectrum of a medium in which optical radiation propagates.

We will use below atmospheric turbulence models taking into account the finiteness of the outer scale of turbulence, namely, the isotropic Karma model [31–34]

$$\Phi_n(\boldsymbol{\kappa},\xi) = 0.033C_n^2(\xi)(\kappa^2+\kappa_0^2)^{-11/6}\exp\left(-\frac{\kappa^2}{\kappa_{\rm m}^2}\right) \tag{53}$$

and the model proposed in Russian publications [36–38]

$$\Phi_n(\boldsymbol{\kappa},\xi) = 0.033C_n^2(\xi)\kappa^{-11/3}\left[1-\exp\left(-\frac{\kappa^2}{\kappa_0^2}\right)\right] \times \exp\left(-\frac{\kappa^2}{\kappa_{\rm m}^2}\right). \tag{54}$$

As shown earlier, the corresponding outer scales for models (53) and (54) are related by a simple numerical coefficient. Therefore, fluctuations of optical characteristics can be calculated with any of these spectra. By using such a spectrum, we obtained expressions [77] for the dispersion of displacements of the energy spectrum of an optical beam and dispersion of fluctuations of the amplitude logarithm (by the smooth-perturbation method). Thus, Russian model (54) gives from (52) (for the condition $\kappa_0^{-1} \gg R$) the expression

$$\left\langle(\boldsymbol{\rho}_F^{\rm pl})^2\right\rangle = 2\pi^2F^2 0.033\Gamma\left(\frac{1}{6}\right)\int_0^X \mathrm{d}\xi\, C_n^2(\xi) \times \left(\frac{R^{-1/3}}{2^{1/6}} - \kappa_0^{1/3}\right). \tag{55}$$

In the case of star jitter in an astronomical telescope, the upper integration limit in (55) should be set equal to ∞. Then, the dispersion of the angular image jitter can be calculated from the expression

$$\frac{\left\langle(\boldsymbol{\rho}_F^{\rm pl})^2\right\rangle}{F^2} = \left\langle(\varphi_F^{\rm pl})^2\right\rangle \approx 3.23R^{-1/3}\int_0^\infty \mathrm{d}\xi\, C_n^2(\xi) \times\left[1-\left(\frac{\kappa_0^2R^2}{2}\right)^{1/6}\right]. \tag{56}$$

We can now use the so-called outer scale of turbulence for the entire atmosphere as a whole [83, 85], introduced, for example, by the expression

$$(\kappa_0^*)^{-1} = \left[\frac{\int_0^\infty \mathrm{d}\xi\, C_n^2(\xi)\kappa_0^{1/3}}{\int_0^\infty \mathrm{d}\xi\, C_n^2(\xi)}\right]^{-3}. \tag{57}$$

Using the coherence radius r_0 of atmospheric turbulence in the form

$$r_0 \approx \left(k^2\int_0^\infty \mathrm{d}\xi\, C_n^2(\xi)\right)^{-3/5}, \tag{58}$$

we can obtain the dispersion of the angular image jitter in the focal lane of a telescope in the form

$$\left\langle(\varphi_F^{\rm pl})^2\right\rangle \approx 3.23R^{-1/3}r_0^{-5/3}k^{-2}\left[1-2^{-1/6}(\kappa_0^*R)^{1/3}\right]. \tag{59}$$

The term in brackets in expression (59) determines the variation in the dispersion of the image dispersion jitter as a function of the receiving aperture size from the $R^{-1/3}$ power dependence.

Table 2 presents the dispersion of the image jitter calculated for different ratios of the effective outer scale for the atmosphere as a whole $(\kappa_0^*)^{-1}$ to the receiving aperture of a telescope R. One can see from Table 2 the strong deviation from the power dependence of the image jitter (59).

Table 2. Deviation in image-jitter dispersion from a power dependence as a function of the telescope aperture.

$(\kappa_0^*R)^{-1}$	1000	300	100	50	30	10	5
$1-2^{-1/6}(\kappa_0^*R)^{1/3}$	0.91	0.87	0.80	0.75	0.70	0.57	0.42

Results presented in Table 2 show that, even when the ratio of the outer scale to the receiving aperture exceeds 10^3, the variation in the behavior of the dispersion of image jitter from a power law $R^{-1/3}$ [4, 14] is considerable, i.e., the influence of the outer scale is observed.

9. Experimental astronomical observations of the manifestation of non-Kolmogorov turbulence

The world's scientific literature contains much data on measuring the effective outer scale from optical and, first and foremost, astronomical observations [78–95, 100–116]. These articles present data obtained with astronomical telescopes analyzing star images or contrast structures in the images of the Sun and Moon. The data show that, as a rule, the outer scale of turbulence increases with height. Several methods for estimating the outer scale, in particular, its integrated value for the vertical propagation, were proposed earlier [100–102]. The use of radiosonde and balloon probing, as well as the interferometric technique and data obtained with wave-front sensors, is described in [105–116].

9.1 Comparison of energy characteristics of Kolmogorov and non-Kolmogorov turbulences

First of all, the influence of the outer scale on the dispersion of temperature (or refractive index) was considered in a number of studies [82, 91–94]. It is known that the energy distribution in the turbulence is determined by the spectral density $\Phi_n(\kappa)$ of refractive-index fluctuations. Because real turbulent inhomogeneities are three-dimensional, an estimate of the dispersion of refractive-index fluctuations should involve the calculation of a functional of the form [19–21, 117, 118]

$$\int_0^\infty \mathrm{d}\kappa\, \kappa^2 \Phi_n(\kappa)\,, \tag{60}$$

where $\Phi_n(\kappa)$ is the spectral density of refractive-index fluctuations in the atmosphere and κ is the spatial wavenumber (or the quantity inverse of the turbulent inhomogeneity).

Note preliminarily that functional (60) is proportional to the dispersion of refractive-index fluctuations. We will calculate this functional for the atmospheric turbulence spectrum [4, 14] assuming its isotropy in the Karman model with the Kolmogorov slope of the spectrum like (54). By calculating integral (60), i.e., the dispersion of refractive-index fluctuations for model (54), we obtain

$$\begin{aligned}\sigma_n^2 &= \int_0^\infty \mathrm{d}\kappa\, \kappa^2 \Phi_n(\kappa) = 0.033 C_n^2 \int_0^\infty \mathrm{d}\kappa\, \kappa^2 (\kappa^2 + \kappa_0^2)^{-11/6} \\ &\times \exp\left(-\frac{\kappa^2}{\kappa_\mathrm{m}^2}\right) = \frac{1}{2} 0.033 C_n^2 \Gamma\left(\frac{3}{2}\right) \kappa_0^{-2/3} \\ &\times \left[\frac{\Gamma(1/3)}{\Gamma(11/6)}\, {}_1F_1\left(\frac{3}{2}, \frac{2}{3}; \frac{\kappa_0^2}{\kappa_\mathrm{m}^2}\right) + \frac{\Gamma(-1/3)}{\Gamma(3/2)} \left(\frac{\kappa_0}{\kappa_\mathrm{m}}\right)^{2/3} \right. \\ &\times \left. {}_1F_1\left(\frac{11}{6}, \frac{4}{3}; \frac{\kappa_0^2}{\kappa_\mathrm{m}^2}\right)\right]. \end{aligned} \tag{61}$$

For the condition $\kappa_0^2 \ll \kappa_\mathrm{m}^2$ for Karman model (54), we have

$$\sigma_n^2 \approx \frac{1}{2}\, 0.033 C_n^2 \Gamma\left(\frac{3}{2}\right) \frac{\Gamma(1/3)}{\Gamma(11/6)}\, \kappa_0^{-2/3}\,. \tag{62}$$

Calculations in (61) give $\sigma_n^2 \propto C_n^2 L_0^{2/3}$, and because, according to model [14], $C_n^2 \propto L_0^{4/3}$, we finally have $\sigma_n^2 \propto L_0^2$.

This means that energy in a turbulent medium depends on the outer scale L_0 of turbulence and therefore knowledge of the outer scale is important for estimates of the turbulence energy. Thus, in our opinion, the outer scale of turbulence is not simply a parameter for fitting measurement data in the low-frequency region of changing parameters of optical waves propagating through a turbulent medium layer: it also determines the total energy of turbulent motion. It is known that a conventional parameter such as the structural constant of the refractive index characterizes the turbulence energy only within the inertial interval, while the coherence radius introduced in [42] gives an estimate of the integrated energy along the propagation path of an optical wave. Then, our studies have shown that the local values of the outer scale of turbulence give an estimate of the turbulence energy within some layer, while the introduced effective outer scale for inhomogeneities from the point of view of the turbulence level in the propagation path characterizes the average turbulence energy, assuming that it is constant along this path.

9.2 Measurements of the coherence radius and effective outer scale of turbulence from astronomical observations

Of interest is the experimental verification of the presence of optical effects in the atmosphere in which the properties caused by the finiteness of the outer turbulence scale are manifested. Numerous recent experimental studies world wide demonstrate deviations of turbulence spectra from the Kolmogorov–Obukhov model not only in the low-frequency region, but also within the inertial interval [118–127]. Of course, to obtain such experimental results, long observations should be performed in the open atmosphere.

One such measurement was performed in the Sayny Mountain region at the Sayny Solar Observatory, Institute of Solar-Earth Physics, Siberian Branch, Russian Academy of Sciences (Mondy, Buryatia). The dispersion σ_α^2 of solar (or lunar) disc-edge jitter was measured with an automated horizontal solar telescope (AST) [77] as a function of the receiving mirror size. The source in experiments was the image of the solar (or lunar) disc edge. The photodetector was a differential photoelectric Brandt sensor for recording the jitter of the image of an extra-atmospheric light source. The Brandt sensor was tested for several ten years and was earlier used for similar studies.

Measurements were performed for five different diameters, 5, 10, 30, 50, and 80 cm, of the receiving mirror (aperture) of the telescope and for two angular sizes of 25$''$ and 10$''$ of the entrance slit of the detector. The zenith angle of the Sun (Moon) position was controlled. Simultaneously with optical measurements, meteorological conditions near the AST were continuously controlled with an ultrasound meteosystem [118]. A few series of experiments were performed in the period from 2009 to 2012. The results of the measurements are presented in Fig. 16.

One can see from Fig. 16 that the standard deviation of the image jitter of the solar disc edge decreases with increasing receiving aperture. Measurements were performed, as a rule, in the evening in the transient turbulent regime. Experiments showed in [18] that the dispersion of displacements of astronomical images for large-aperture detectors weakly depends on the aperture, unlike the usual dependence, when the dispersion for the Kolmogorov spectrum depends on the receiving aperture $\sim a_\mathrm{t}^{-1/3}$. Data in Fig. 16 allow us to estimate the coherence radius and the effective outer scale $(\kappa_0^*)^{-1}$ for the entire atmosphere. The integrated atmospheric scales r_0 and $(\kappa_0^*)^{-1}$ can be simultaneously measured from expression (59). In addition, measurements of image jitter in experiments should be performed for at least two values of the receiving aperture to obtain two parameters characterizing the atmosphere: r_0, determined from (58), and $(\kappa_0^*)^{-1}$, determined from (57). Table 2 presents the calculated sensitivities of this method.

Finally, the results of measurements lead to the following conclusions:

(i) Ignoring the influence of the outer scale of turbulence in measurements of the coherence radius r_0 from the image jitter in the telescope focus overstates its measured values by approximately 10–25%.

(ii) Using data in Fig. 16 (for any pair of points on curves), the effective outer scale $(\kappa_0^*)^{-1}$ can be estimated for the entire atmosphere. Its value proved to be from 12 to 35 m, which does not contradict our model calculations.

(iii) As a whole, measurements performed at the Sayan Solar Observatory gave an effective outer scale of turbulence

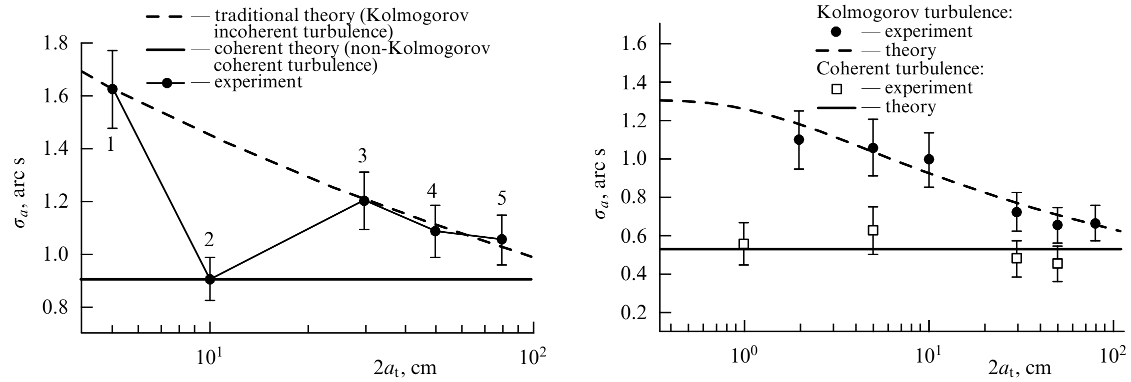

Figure 16. Root-mean-square deviation σ_a^2 of the astronomical image jitter of the solar disc edge as a function of the telescope entrance aperture diameter. Sayan Solar Observatory. 2010 and 2011 summer measurements [116–118].

between 8 and 12 m and the corresponding coherence radius (according to Fried) of 25 to 41 mm.

9.3 World experience in measurements and estimates of the outer scale of turbulence from astronomical observations

The most reliable and complete experimental data on estimates of the outer scale of turbulence were obtained in astronomical observations. Below, we consider astronomical data used to estimate the effective outer scale for the atmosphere as a whole.

The first attempt to estimate this outer scale was made by Mariotti and coauthors [103] at Observatoire Plateau de Calern, France, who used a 12T interferometer to obtain the outer scale equal to 8 m. A few years later, Colavita and coauthors [53] obtained the outer scale at more than 2 km in measurements with a stellar Mark III interferometer. Using the same interferometer, Buscher and coauthors [101] estimated this scale as only 30 m. The measurements of fluctuations of arrival angles with the help of Shack–Hartmann sensors give an output scale in the range from 5 to 8 m [105]. Experiments [104, 106] performed with the Come-On electro-optical system gave the outer scale value of about 50 m. Using a modified Differential Image Motion Monitor (DIMM), Ziad at al. [107] estimated this parameter at a value from 5 to 100 m. Preliminary experiments performed with a Grating Scale Monitor at two French laboratories, Observatoire de Nice and Observatoire Plateau de Calern [108], gave the outer scale in the range from 5 to 300 m. Later, measurements were performed with a Generalized Seeing Monitor (GSM) at the world's main observatories: La Silla, Maidanak, Cerro Tololo, Paranal, Roque de los Muchachos, Mauna Kea, Mount Palomar, and Dome C. These measurements, except those at the Dome C Observatory, gave the outer scales of turbulence in the range from 12 to 50 m [109, 110].

Note that, according to Ziad's opinion, all the methods mentioned above are model-dependent, which means that experimental data are analyzed assuming the applicability of the Kolmogorov spectral model or models like (26) and (28). On the other hand, an estimate of the local outer scale can be obtained from measurement data, as in [111] and [112]. Note that all these measurements give a local value of the outer scale of no more than 5 m. Such a large difference between local values and the effective outer scale for the entire atmosphere (according to astronomical data) is explained by the different definition of the latter. Indeed, GSM measurements performed at the Gemini South Observatory [113] in October 1998 gave the effective outer scale approximately 13–16 times greater than its local value near Earth. This result is explained by the use of different definitions of the outer scale in different measurement methods. At the same time, meteorological data and predictive models can be successfully used for estimates of the outer scale [114, 115].

Note that a comparative analysis [107] of experimental data accumulated world wide was performed for the first time by the author of this review in [95]. Table 3 is taken from [95].

As a whole, the values of the effective outer scale obtained in these experiments agree well with the results of different optical measurements (see Fig. 16) and with the model calculations presented in Section 3. Nevertheless, we will

Table 3. Observed values of the effective outer scale of turbulence.

Data publication year	References	Effective outer scale, m	Astronomical device used	Experiment location
1983	Lukin et al. [79]	3 – 15	TT-600	SAO RAS*
1984	Mariotti et al. [103]	8	I2T	CERGA**
1987	Colavita et al. [53]	> 2000	Mark III	Mount Wilson
1989	Tallon et al. [105]	5 – 8	Hartmann-Shack	Mauna Kea
1991	Rigaut et al. [106]	< 50	Come-On	La Silla
1991	Rousset et al. [104]	> 2	DIMM	Roque de los Muchachos
1993	Ziad et al. [107]	5 – 100	Shack-Hartmann	OHP***
1994	Agabi et al. [108]	50 – 300	GSM1	OCA****
1995	Buscher et al. [104]	10 – 100	Mark III	Mount Wilson
1995	Fuchs [112]	2.4 – 1.5	Ballons	Paranal

* Special Astrophysical Observatory, RAS.
** Centre de recherches en geodynamique et astrometrie.
*** Observatoire de Haute-Provence.
**** Observatoire de la Cote d'Azur.

point out here a considerable difference between our concept of the outer scale [96–98], which is presented is this review, and the approach to the estimate of this parameter in [107–110]. Recent studies [118–127] demonstrate significant deviations in turbulence spectra in the atmosphere from the Kolmogorov model, even in the inertial interval. This forces researchers to introduce turbulence spectra of different types, significantly different from traditional spectra, into models in calculations of parameters of optical systems, including adaptive-optics systems [126–132].

Model calculations based on turbulence spectra with a finite outer scale have long been applied for calculating parameters of future astronomical telescopes using adaptive optics. Thus, the potential parameters of a Euro50 — project of large European astronomical telescope were analyzed in [133] using the seven-layer model of the atmosphere for the Roque de los Muchachos Observatory, Canary Islands [59]. The effective outer scale for the model was directly calculated by (48) using the vertical profile of C_n^2 and some assumptions about the vertical distribution of L_0 in the interval of 20–40 m, including the turbulence of the boundary atmospheric layer [59]. It was found that the variation in the effective outer scale considerably changes the balance between the global slope of the wave front and its higher aberrations. Calculations similar to [33] were successfully used in [105–115] to estimate the efficiency of the application of astronomical telescopes in different regions of the world.

10. Conclusions

Numerous measurements in the atmosphere have shown that the spectral density of refractive-index fluctuations in the energy interval, unlike that in the inertial interval of wavenumbers, is no longer a universal function. It is known that the low-frequency spectrum depends both on the underlying-surface profile (for small heights) and on weather conditions. Naturally, the spectrum shape will change, for example, with changing height above the underlying surface and with variations in the thermodynamic stability of turbulence. Therefore, the assumption about the local homogeneity and isotropy of turbulence is no longer fulfilled. At the same time, calculating statistical characteristics of optical waves (estimates of the dispersion of fluctuations) requires simple and convenient spectral models.

Experiments on horizontal paths have shown that the value of the outer scale is comparable to the propagation height of optical radiation above the underlying surface; however, these values are different for different authors. This can be explained by the fact that the real atmosphere contains, along with small-scale turbulence (no more than a few meters in size), larger-scale motions of a different nature. These motions can be caused by the radiation variegation of the underlying surface, the screening of the underlying surface by cloudy structures, and some other factors. Such large-scale formations can be considered in the ground-level layer as slow variations in external conditions determining the generation of small-scale turbulence. Note that parameters of the turbulence (and model) of the ground-level layer should change in time (and space) with the characteristic scale of these large-scale structures.

Thus, if a model parameter such as the outer scale was selected from synchronous measurements of fluctuations of some optical parameter and the turbulence intensity, these measurements should be accompanied by measurements of average meteoparameters: the temperature and wind-velocity gradients, the transverse component of the wind velocity at the propagation height of optical radiation, and the dispersion of fluctuations of the wind velocity.

Experiments performed in the atmosphere have shown that:

(i) the outer scale of turbulence in the ground-level atmospheric layer is comparable to the

(ii) the outer scale of turbulence depends on the thermodynamic stability of the atmosphere;

(iii) the largest large-scale inhomogeneities of the atmospheric turbulence in the ground-level atmospheric layer have anisotropic properties. This can be manifested in the inequality of outer scales in the vertical and transverse directions;

(iv) the vertical distribution of atmospheric inhomogeneities shows that the atmosphere has a layer-homogeneous structure;

(v) as the height above the underlying surface increases, the outer scale increases and can reach 30–50 m in the open atmosphere.

Numerous studies show that the behavior of the turbulence spectrum in the low-frequency region in the ground-level layer can no longer be described by a single parameter — the turbulence intensity (it is assumed that the behavior of the spectrum in this region is not universal). It is necessary to take into account in calculations that the assumption about the local isotropy for large-scale inhomogeneities close to the outer scale of turbulence is not correct enough for real atmospheric conditions.

Nevertheless, fluctuations in optical fields (for example, statistical characteristics of phase fluctuations of optical waves) were calculated using different models describing the spectrum in the large-scale region. These models already had two parameters, the second one being the so-called outer scale. Calculations used different models of the turbulence spectrum, the coincidence of experimental data with calculations being achieved by selecting the outer scale. In turn, the outer scale of turbulence determines in fact the energy characteristics of turbulent fluctuations.

Acknowledgments

This study was supported by the AAAA-A17-117021310146-3 project. The author thanks his colleagues N N Botygina, L A Bol'basova, O N Emaleev, V V Nosov, E V Nosov, and A V Torgaev their for collaboration over many years, on which this review is based.

References

1. Zuev V E *Rasprostranenie Lazernogo Izlucheniya v Atmosfere* (Propagation of Laser Radiation in Atmosphere) (Moscow: Radio i Svyaz', 1981)
2. Zuev V E et al. *Lazernoe Zondirovanie Industrial'nykh Aerozolei* (Laser Probing of Industrial Aerosols) (Novosibirsk: Nauka, 1986)
3. Tatarskii V I *Rasprostranenie Voln v Turbulentnoi Atmosfere* (Propagation of Wave in Turbulent Atmosphere) (Moscow: Nauka, 1967)
4. Gurvich A S et al. *Lazernoe Izluchenie v Turbulentnoi Atmosfere* (Lase Radiation in Turbulent Atmosphere) (Moscow: Nauka, 1976)
5. Rytov S M, Kravtsov Yu A, Tatarskii V I *Principles of Statistical Radiophysics* Vol. 2 *Elements of Random Fields* (Berlin: Springer-Verlag, 1989); Translated from Russian: *Vvedenie v Statisticheskuyu Radiofiziku. Sluchainye Polya* Ch. 2 (Moscow: Nauka, 1978)
6. Zuev V E, Banakh V A, Pokasov V V *Optika Turbulentoi Atmosfery* (Optics of Turbulent Atmosphere) (Optics of Turbulent Atmosphere. Modern Problems of Atmospheric Optics, Vol. 5) (Leningrad: Gidrometeoizdat, 1988)

7. Tatarskii V I *Izv. Akad. Nauk SSSR, Geofiz.* (6) 689 (1956)
8. Gur'yanov A E, in *Trudy Vsesoyuznoi Konf. Rabochei Gruppy 'Astroklimat' Astrosoveta AN SSSR, Abastumani, 1981. Astroklimat i Effektivnost' Teleskopov* (Proc. of the All-Union Conf. of the Astroclimate Working Group, Astroboard, USSR Academy of Sciences, Abastumani, 1981. Astroclimate and the Efficiency of Telescopes) (Leningrad: Nauka, 1984) p. 164
9. Monin A S, Yaglom A M *Statistical Fluid Mechanics*; *Mechanics of Turbulence* Vol. 1 (Cambridge, MA: MIT Press, 1971); Translated from Russian: *Statisticheskaya Gidromekhanika* Vol. 1 (St. Petersburg: Gidrometeoizdat, 1992); Monin A S, Yaglom A M *Statistical Fluid Mechanics*; *Mechanics of Turbulence* Vol. 2 (Cambridge, MA: MIT Press, 1975); Translated from Russian: *Statisticheskaya Gidromekhanika*, Vol. 2 (St. Petersburg: Gidrometeoizdat, 1996)
10. Monin A S, Obukhov A M *Trudy Geofiz. Inst. Akad. Nauk SSSR* **24** (151) 163 (1954)
11. Obukhov A M *Izv. Akad. Nauk SSSR. Geogr. Geofiz.* **13** 58 (1949)
12. Obukhov A M *Izv. Akad. Nauk SSSR. Geogr. Geofiz.* **5** 453 (1941)
13. Obukhov A M, Yaglom A M *Prikl. Matem. Mekh.* **15** (1) 3 (1951)
14. Tatarskii V I *Teoriya Fluktuatzionnykh Yavlenii pri Rasprostranenii Voln v Turbulentnoi Atmosfere* (Theory of Fluctuation Phenomena During the Propagation of Waves in the Turbulent Atmosphere) (Moscow: Izd. AN SSSR, 1959)
15. Reynolds O *Proc. R. Soc. Lond.* **35** 84 (1883)
16. Reynolds O *Proc. R. Soc. Lond.* **56** 40 (1894)
17. Taylor G I *Proc. R. Soc. Lond. A* **151** 421 (1935); *Proc. R. Soc. Lond. A* **156** 307 (1936)
18. Taylor G I *Proc. Roy. Soc. Lond. A* **164** 476 (1938)
19. Kolmogorov A N *Dokl. Akad. Nauk SSSR* **30** (4) 299 (1941)
20. Kolmogorov A N *Dokl. Akad. Nauk SSSR* **31** (6) 538 (1941)
21. Kolmogorov A N *Dokl. Akad. Nauk SSSR* **32** (3) 19 (1941)
22. Kolmogorov A N *Izv. Akad. Nauk SSSR, Fiz.* **6** (1–2) 56 (1942)
23. Golitsyn G S *Prikl. Matem. Mekh.* **24** 1124 (1960)
24. Karman T *Aerodynamics* (New York: McGraw-Hill, 1963)
25. Obukhov A M *Izv. Akad. Nauk SSSR. Geofiz.* 2 155 (1953)
26. Gurvich A S *Izv. Akad. Nauk SSSR. Fiz. Atmos. Okeana* **4** (2) 160 (1963)
27. Time N S *Izv. Akad. Nauk SSSR. Fiz. Atmos. Okeana* **8** (1) 90 (1972)
28. Kalistratova M A, Pokasov V V *Izv. Vyssh. Uchebn. Zaved. Radiofiz.* **15** (2) 723 (1972)
29. Emaleev O N et al. "Sledyashchii tsifrovoi fazometr opticheskogo diapazona" ("Tracking digital optical phasemeter"), Authors' Certificate No. 397852. Bull. no. 37, 17.11.1973
30. Lukin V P, Pokasov V V, Khmelevtsov S S *Radiophys. Quantum Electron.* **15** 1426 (1972); *Izv. Vyssh. Uchebn. Zaved. Radiofiz.* **15** (12) 1861 (1972)
31. Lukin V P, Pokasov V V, Khmelevtsov S S *Izv. Vyssh. Uchebn. Zaved. Radiofiz.* **16** 1726 (1973)
32. Mironov V L et al. *Izv. Akad. Nauk SSSR. Radiotekh. Elektron.* **20** 6 1164 (1975)
33. Bouricius G M B, Clifford S F *J. Opt. Soc. Am.* **60** 1484 (1970)
34. Consortini A, Ronchi L, Moroder E *J. Opt. Soc. Am.* **63** 1246 (1973)
35. Gel'fer E I, Kon A I, Cheremukhin A N *Izv. Vyssh. Uchebn. Zaved. Radiofiz.* **16** 245 (1973)
36. Kon A I *Izv. Vyssh. Uchebn. Zaved. Radiofiz.* **15** 533 (1972)
37. Mironov V L et al. *Izv. Akad. Nauk SSSR. Radiotekh. Elektron.* **20** 1164 (1975)
38. Lukin V P et al. *Izv. Vyssh. Uchebn. Zaved. Fiz. Atmos. Okeana* **12** 550 (1976)
39. Zilitinkevich S S *Izv. Akad. Nauk SSSR. Fiz. Atmos. Okeana* **7** 1201 (1971)
40. Lukin V P *Izv. Vyssh. Uchebn. Zaved. Fiz.* (9) 100 (1976)
41. Turchin V F, Kozlov V P, Malkevich M S *Sov. Phys. Usp.* **13** 681 (1971); *Usp. Fiz. Nauk* **102** 345 (1970)
42. Fried D L *TIIER* **55** (1) 19 (1967)
43. Mironov V L et al. *Izv. Akad. Nauk SSSR. Fiz. Atmos. Okeana* **12** 550 (1976)
44. Lukin V P et al. *Izv. Akad. Nauk SSSR. Fiz. Atmos. Okeana* **13** (1) 90 (1977)
45. Turchin V P, Nozil V Z *Izv. Akad. Nauk SSSR. Fiz. Atmos. Okeana* **5** (1) 29 (1969)
46. Turchin V F, Turovtseva L S *Opt. Spektrosk.* **36** (2) 280 (1974)
47. Time N S, Turovtseva L S, Preprint No. 89 (Moscow: Keldysh Institute of Applied Mathematics, USSR Acad. of Sci., 1973) Dep. VINITI 1227
48. Gurvich A S et al. *Izv. Akad. Nauk SSSR. Fiz. Atmos. Okeana* **10** 484 (1974)
49. Zubkovskii S L Koprov B M *Izv. Akad. Nauk SSSR. Fiz. Atmos. Okeana* **5** 323 (1969)
50. Kaimal J C, Wyngaard J C *Quart. R. Meteor. Soc.* **98** (414) 563 (1972)
51. Strohbehn J W *J. Geoph. Res.* **75** (6) 23 (1970)
52. Coulman C E et al. *Appl. Opt.* **27** (1) 155 (1988)
53. Colavita M M *Appl. Opt.* **26** (12) 4106 (1987)
54. Greenwood D P, Tarazano D O *J. Opt. Soc. Am. A.* **25** (6) 1349 (2008)
55. "Site Testing for the VLT", VLT Report 60 (Munchen: ESO, 1990)
56. Lukin V P, Pokasov V V *Appl. Opt.* **20** 121 (1981)
57. Kon A I *Izv. Vyssh. Uchebn. Zaved. Radiofiz.* **13** (1) 61 (1970)
58. Tokovinin A, Travouillon T *Mon. Not. R. Astron. Soc.* **365** 1235 (2006)
59. Muñoz-Tuñón C, Varela AM, Garcia Lorenzo B "Instruments and tools for site testing", GW3-ESO- Site Evaluation (2006)
60. Beland R R, in *The Infrared and Electro-Optical Systems Handbook* Vol. 2 (Exec. Eds J S Accetta, D L Shumaker) (Bellingham, WA: SPIE Optical Engineering Press, 1993) Ch. 2
61. Magee P "A toolbox for atmospheric propagation modeling user's guide version 4.1.455", MZA Associates Corporation, March 13 (2007)
62. Roddier F et al. *Proc. Soc. Photo-Opt. Instrum. Eng.* **1236** 485 (1990)
63. "Very Large telescope. The Paranal model atmosphere for adaptive optics", Doc. No. VLT-TRE-ESO-11630-1137. Is.1.0 (1996)
64. Kopeika N, Middle N S *Proc. SPIE* **5793** 89 (2005)
65. Obukhov A M *Izv. Akad. Nauk SSSR, Geofiz.* 9 17 (1960)
66. Gurvich A S, Gracheva M E *Izv. Akad. Nauk SSSR. Fiz. Atmos. Okeana* **16** 1107 (1980)
67. Lukin V P *Opt. Atmos. Okeana* **5** (4) 354 (1992)
68. Lukin V P *Proc. SPIE* **1968** 327 (1993)
69. Lukin V P *Opt. Atm. Okeana* **5** (12) 1294 (1992)
70. Lukin V P *Proc. SPIE* **2200** 384 (1994)
71. Lukin V P *Opt. Atmos. Okeana* **6** (9) 628 (1993)
72. Lukin V P *Proc. SPIE* **2222** 527 (1994)
73. Lukin V P *Opt. Atmos. Okeana* **17** (12) 1028 (2004)
74. Voitsekhovich V, Cuevas S *J. Opt. Soc. Am. A* **12** 2523 (1995)
75. Lukin V P, Sazanovich V M *Izv. Akad. Nauk SSSR. Fiz. Atmos. Okeana* **14** 996 (1978)
76. Lukin V P et al, in *Rasprostranenie Opticheskikh Voln v Sluchaino-neodnorodnoi Atmosfere* (Propagation of Optical Waves in the Random Atmosphere) (Ed. V E Zuev) (Novosibirsk: Nauka, 1979)
77. Lukin V P et al. *Izv. Vyssh. Uchebn. Zaved. Radiofiz.* **23** 721 (1980)
78. Emaleev O N, Lukin V P, Potanin S F, in *Proc. of the V All-Russian Symp. on Laser Radiation Propagation in the Atmosphere* Pt. 2 (Tomsk, 1979) p. 144
79. Gubkin S M et al. *Sov. Astron.* **27** 455 (1983); *Astron. Zh.* **60** (4) 789 (1983)
80. Lukin V P *Proc. SPIE* **2471** 347 (1995)
81. Antoshkin L V et al. *Opt. Atmos. Okeana* **8** (12) 1784 (1995)
82. Coulman C E, Vernin J *Appl. Opt.* **30** (1) 118 (1991)
83. Lukin V P, Nosov E V, Fortes B V, in *Tezisy Dokladov III Mezhrespublikanskogo Simpoziuma Optika Atmosfery i Okeana* (Proc. of the 3rd Interrepublic Symp. on Optics of Atmosphere and Ocean) (Tomsk, 1996) p. 31
84. Fried D L *J. Opt. Soc. Am.* **56** 1380 (1966)
85. Lukin V P, Nosov E V, Fortes B V *Opt. Atmos. Okeana* **10** (2) 162 (1997)
86. Lukin V P, Nosov E V, Fortes B V *Proc. SPIE* **3219** 98 (1998)
87. Borgnino J *Appl. Opt.* **29** 1863 (1990)
88. Borgnino J, Martin F, Ziad A *Opt. Commun.* **91** 267 (1992)
89. Ziad A et al. *Astron. Astrophys.* **282** 1021 (1994)
90. Lukin V *ASP Conf. Ser.* **266** 18 (2002)
91. Vernin J *ASP Conf. Ser.* **266** 2 (2002)
92. Dewan E M, Grossbard N *Environ Fluid Mech.* **7** 383 (2007)
93. Reinhard GW, Collins S A *J. Opt. Soc. Am.* **62** 1526 (1972)
94. Coulman C E et al. *Appl. Opt.* **27** 155 (1988)
95. Lukin V P *Opt. Atmos. Okeana* **8** 479 (1995)

96. Lukin V P *Opt. Atmos. Okeana* **8** 455 (1995)
97. Lukin V P, Fortes B V *Pure Appl. Opt.* **5** (1) 1 (1996)
98. Lukin V P, Fortes B V *Astron. Rep.* **40** 378 (1996); *Astron. Zh.* **73** 419 (1996)
99. Bol'basova L A et al. *Opt. Atmos. Okeana* **25** 845 (2012)
100. Sarazin M, Roddier F *Astron. Astrophys.* **227** 1360 (1987)
101. Buscher D F et al. *Appl. Opt.* **34** 1081(1995)
102. Tokovinin A *Proc. SPIE* **3353** 1155 (1998)
103. Mariotti J M, Di Benedetto G P *Proc. Int. Astron. Union Colloq.* **79** 257 (1984)
104. Rousset G, Madec P-Y, Rabaud D, in *ESO Conf. on High-Resolution Imaging by Interferometry II, Ground-Based Interferometry at Visible and Infrared Wavelengths, 15–18 October 1991, Garching bei München, Germany, Proc.* (ESO Conf. and Workshop Proc., Vol. 39, Eds J M Beckers, J M Merkle) (Garching bei München: European Southern Observatory, 1992) p. 1095
105. Tallon M, Thèse de doctorat (Nice: de l'Université de Nice, 1989)
106. Rigaut F et al. *Astron. Astrophys.* **250** 280 (1991)
107. Ziad A et al. *Astron. Astrophys.* **282** 1021 (1994)
108. Agabi A et al. *Astron. Astrophys. Suppl. Ser.* **109** 557 (1995)
109. Ziad A et al. *Appl. Opt.* **39** 5415 (2000)
110. Ziad A *Proc. SPIE* **9909** 99091K (2016)
111. Coulman C E et al. *Appl. Opt.* **27** 155 (1988)
112. Fuchs A, Thèse de doctorat (Nice: Université de Nice, 1995)
113. Abahamid A et al. *Astron. Astrophys.* **416** 1193 (2004)
114. Masciadri E, Vernin J, Bougeault P *Astron. Astrophys. Supppl. Ser.* **137** 185 (1999)
115. Giordano C, Thèse de doctorat (Nice: de l'Université de Nice-Sophia-Antipolis, 2014)
116. Lukin V P *Proc. SPIE* **5981** 1 (2005)
117. Lukin V P et al. *Usp. Sovr. Estestvoznan* (12) Pt. 4 369 (2014)
118. Lukin V P *Proc. SPIE* **09680** (2015)
119. Tofsted David H *Opt. Eng.* **53** 044112 (2014)
120. Toselli I, Beason M, in *Workshop on Non-Kolmogorov Turbulence and Associated Phenomena, Ettlingen, 01–03.07.2019*
121. Velluet Marie-Thérèse, in *Workshop on Non-Kolmogorov Turbulence and Associated Phenomena, Ettlingen, 01–03.07.2019*
122. Charnotskii M, in *Workshop on Non-Kolmogorov Turbulence and Associated Phenomena, Ettlingen, 01–03.07.2019*
123. Italo Toselli, Szymon Gladysz, Imaging and Applied Optics © 2014 OSA. PM3E.6.pdf
124. Wenhe D et al. *J. Russ. Laser Res.* **35** 416 (2014)
125. Gladysz S *Proc. SPIE* **09614** 961402 (2015)
126. Bol'basova L A, Lukin V P, Nosov V V *Appl. Opt.* **53** (10) B231 (2014)
127. Linyan C *Optik* **154** 473 (2018)
128. Charnotskii M, Brennan T *Proc. SPIE* **10408** 104080L (2017)
129. Charnotskii M *J. Opt.* **20** 025602 (2018)
130. Charnotskii M, in *Workshop on Non-Kolmogorov Turbulence and Associated Phenomena, Ettlingen, 01–03.07.2019*
131. Basu S, in *Workshop on Non-Kolmogorov Turbulence and Associated Phenomena, Ettlingen. 01–03.07.2019*
132. Roggemann Michael C, Imaging and Applied Optics © 2014 OSA. PM3E.1.pdf